

# CENN: Conservative energy method based on neural network with subdomains for solving heterogeneous problems involving complex geometries

Yizheng Wang<sup>a</sup>, Jia Sun<sup>a</sup>, Xiang Li<sup>b</sup>, Yinghua Liu<sup>a,\*</sup>

<sup>a</sup>*School of Aerospace Engineering, Tsinghua University, Beijing 100084, China*

<sup>b</sup>*School of Information Science and Technology, Hainan Normal University, Haikou 570206, China*

---

## Abstract

We propose a conservative energy method based on a neural network with subdomains (CENN), where the admissible function satisfying the essential boundary condition without boundary penalty is constructed by the radial basis function, particular solution neural network, and general neural network. The loss term at the interfaces has the lower order derivative compared to the strong form PINN with subdomains. We apply the proposed method to some representative examples to demonstrate the ability of the proposed method to model strong discontinuity, singularity, complex boundary, non-linear, and heterogeneous PDE problems. The advantage of the method is the efficiency and accuracy compared to the strong form PINN. It is worth emphasizing that the method has a natural advantage in dealing with heterogeneous problems.

**Keywords:** Physics informed, Deep energy method, Domain decomposition, Interface problem, Complex geometries, Deep neural network

---

## 1. Introduction

Many physical phenomena are modeled by partial differential equations. In general, it is difficult to obtain the analytical solutions of partial differential equations. So we often use various numerical methods to obtain the approximate solutions in a finite dimensional space, such as the finite element method, the finite difference method, the finite volume method, and mesh-free method, and so on [1]. These traditional numerical methods have been fully developed in the past decades. The traditional methods are computationally efficient and accurate for engineering applications, especially the finite element method. However, the finite element method often faces dimensional explosion and distortion problems for the high-dimensional problems, making the efficiency exponentially lower [2]. In addition, meshing is often difficult for the problems with complex geometries [3]. The traditional method requires the selection of specific basis functions to construct the approximation function, such as the singular element specifically designed for fracture mechanics singularities [4] in the finite element method. Constructing basis functions corresponding to different elements undoubtedly increases the brainpower cost.

Artificial intelligence has impacted many fields in the last decade, and it is now generally believed that the means to achieve artificial intelligence can be machine learning, using data-driven optimization. Deep learning, a method in machine learning, has achieved unprecedented success in computer vision [5], speech recognition [6], natural language processing [7], strategy games [8, 9], drug development [10] and, so on. The success of deep learning partially attributes to the powerful approximation capabilities of the neural network [11]. It can be said that deep learning is everywhere, empowering various fields. It is natural to use the neural network as the approximation function of partial differential equations, i.e., physical informed neural network (PINN) [12].

The idea of using the neural network to solve PDEs has been pursued in the last century [13], but it has not received enough attention due to hardware limitations. Raissi et al have dealt with the strong form of the

---

\*Corresponding author

Email addresses: wang-yz19@mails.tsinghua.edu.cn (Yizheng Wang), yhliu@tsinghua.edu.cn (Yinghua Liu)

PDE, i.e., a weighted residual method with neural networks as the approximate function [12]. PINN combines the differential equations in the domain, boundary conditions, and initial conditions into the loss function by weighted summation. Different choices of trial function and test function correspond to various numerical methods, eg. trial function with domain decomposition [14] and test function with domain decomposition [15]. The advantage of PINN strong form is that it is less dependent on sampling size, only requiring zero loss at any given coordinate point [16]. Since all partial differential equations have a weighted residual form, the strong form is general and can almost solve any partial differential equation. Another way of PINN is the deep energy form [16, 17, 18, 19, 20, 1], use the physical potential energy as the optimized loss function. The advantage of this deep energy method (DEM) is that the physical interpretability is stronger than PINN strong form. In addition, the hyperparameters are less than strong form. Because the highest derivative order is smaller than the strong form, the computational efficiency and accuracy are higher. The disadvantage of DEM is that it depends on the choice of the integration scheme for the energy integration as exactly as possible [16, 17]. The generality is not good as the strong form, because not all partial differential equations have a corresponding energy form [4].

Most of the current research is focused on the strong form of PINN, the research about the energy form is relatively little. The strong form of PINN has too many hyperparameters, especially CPINN [14]. We often need to adjust hyperparameters empirical [16, 17]. Although there are currently the valuable research results [21, 22, 23, 24] for the selection of hyperparameters, but the optimal hyperparameters still do not know when faced with specific problems. On the other hand, the possible displacement field in the DEM is often constructed by a penalty function [20], or by multiplying coordinates [1, 19]. In [3, 17], the possible displacement field is constructed by distance network and particular solution network, but lacks PINN energy form with subdomains.

In this work, we propose a conservative energy form based on neural networks with subdomains (CENN), where the admissible function is constructed by the radial basis function(RBF), particular solution neural network, and general neural network. This method of constructing the admissible function is suitable for the complexity boundary problem. This is perhaps the first attempt to leverage the power of PINN energy form to the heterogeneous problem including discontinuity, singularity, high-order multi-physics, and multi-field nonlinear PDE problem. The advantages of the CENN are multi-fold :

- **Efficient handling of heterogeneous problems:** Unlike traditional DEM, CENN can handle the discontinuity solution and derivative discontinuity problem on the interface by assigning the different neural networks in each subdomain. It is worth noting that the interface loss in CPINN, has more terms than CENN , which will be mentioned in detail in Section 3.
- **Penalty less:** CENN only has the interface hyperparameter, unlike strong form. Compared to CPINN, CENN can produce more accurate solutions with fewer unknowns hyperparameters to reduce the cost of adjusting hyperparameters.
- **Accuracy and efficiency:** Due to the lower derivative in CENN, the accuracy and efficiency are higher than the strong form. In addition, the partial independence between the subdomains can be implemented by a parallelization algorithm, which will further improve efficiency.
- **Less brainpower cost:** CENN benefits from the expressive power of the neural network. So we need not construct the approximation function by designing a basis function, e.g. the special elements in the finite element method.
- **Feasibility of high-dimensional problems and distortion problems:** CENN is a mesh-free method, so it has the same advantage as the mesh-free method. The proposed algorithm is quite effective in high dimensions and distortion.
- **Flexibility of the subdomains configuration:** CENN can divide the region to different neural networks. The different configurations, such as the number of hidden layers, activation function, and so on, can be assigned to the different neural networks for the specific problems.

The outline of the paper is as follows. In Section 2, we introduce some preparatory knowledge to warm up. It provides a brief introduction to feed-forward neural network, PINN, and the DEM. Section 3 gives the

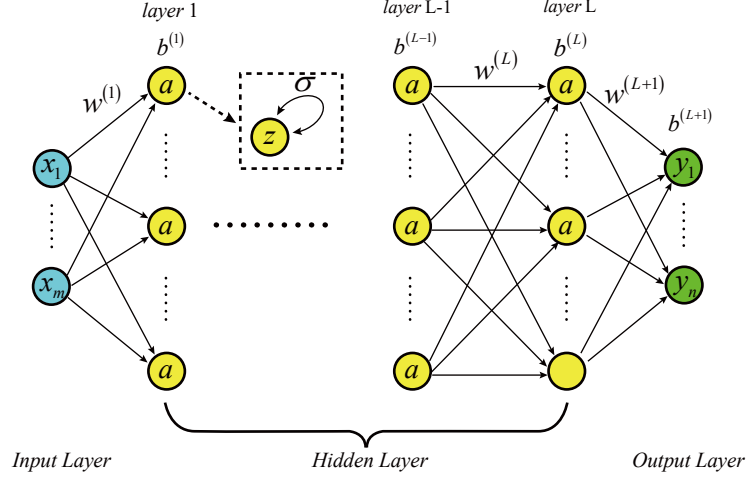


**Fig. 1.** Schematic of fully neural network, blue circle in the Neural network is the inputs. Yellow circle in the Neural network is the hidden neurons. Green circle in the neural network is the output neurons.  $x$  and  $y$  are the input and output.  $z$  is the linear output.  $\sigma$  is the activation function acting on  $z$ .

methodology of the proposed method CENN. The strategy for constructing the admissible function based on the radial basis function and particular network is explained. Section 4 shows some representative applications :

1. The crack problem shows the proposed method can tackle the strong discontinuity and singularity problem, where various comparisons are made between data-driven, CPINN, and CENN.
2. The complex boundary and heterogeneous problem shows the proposed method has the feasibility of complex boundary and derivative discontinuity problems, where various comparisons are made between CPINN, DEM and, CENN.
3. The non-linear hyperelasticity problem with composite material proves the proposed method can deal with non-linear PDE, where various comparisons are made between FEM, DEM, and CENN.

Section 5 shows the discussion. Finally, Section 6 concludes the study by summarizing the key results of the present work.

## 2. Preparatory knowledge

In this section, we provide an overview of the feed-forward neural network. Next, we introduce the main idea of the PINN. In the end, we give an outline of the deep energy method (DEM).

### 2.1. Introduction to feed-forward neural network

The feed-forward neural network is a multiple linear regression with the activation function aimed to increase the non-linear ability. Fig. 1 shows the schematic of feed-forward neural network. The fully neural network algorithm is given by

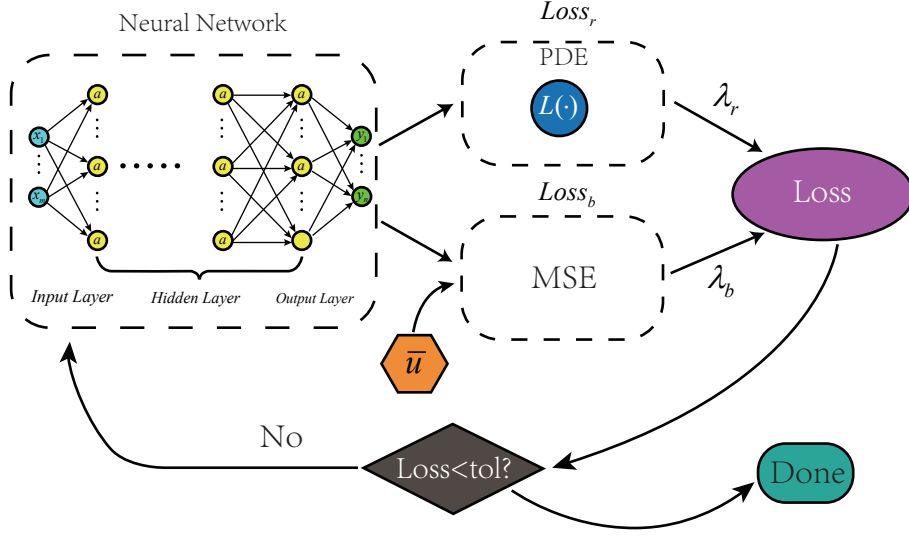


**Fig. 2.** Schematic of PINN, blue circle in the Neural network is the inputs. Yellow circles in the Neural network is the hidden neurons. Green circles in the neural network is the output neurons.  $L(\cdot)$  is the differential operator related to the PDE.  $\bar{u}$  is the given data including boundary and the initial condition. MSE is the mean square error to constant the interesting field to satisfy the essential boundary.  $\lambda_r$  and  $\lambda_b$  are the weight of the residual Loss and the boundary Loss(including initial condition if temporal problem) respectively.

$$\begin{aligned}
 z^{(1)} &= w^{(1)}x + b^{(1)} \\
 a^{(1)} &= \sigma(z^{(1)}) \\
 &\vdots \\
 z^{(L)} &= w^{(L)}a^{(L-1)} + b^{(L)} \\
 a^{(L)} &= \sigma(z^{(L)}) \\
 y &= w^{(L+1)}a^{(L)} + b^{(L+1)}
 \end{aligned} \tag{1}$$

where  $z^{(l)}$  is the linear transformation of the previous neurons  $a^{(l-1)}$ , the layers  $1 \leq l \leq L$  are the hidden layers.  $a^{(l)}$  is the output of  $z^{(l)}$  through the activation function  $\sigma$ , and the activation function  $\sigma$  is a non-linear function, such as tanh, sigmoid, and so on. In this article, we uniquely use the tanh function as the activation function

$$\tanh = \frac{e^x - e^{-x}}{e^x + e^{-x}}. \tag{2}$$

where  $w^{(m)}$  is the weight between the layer m-1 and m.  $b^{(m)}$  is the bias of the layer m.

## 2.2. Introduction to Physical-Informed Neural Network

In this section, we give an outline of Physical-Informed Neural Network(PINN). The overall process of the PINN is shown in Fig. 2. PINN uses a neural network as the approximation function. PDE formulas related to the specific problem are the guide of the loss function construction. The necessary data including the bound and initial conditions is required in advance. The  $Loss_b$  is the discrepancy between the necessary data(boundary and initial condition) and neural network approximation, which commonly uses MSE as the criterion to constant the interesting field to satisfy the essential boundary. Then the  $Loss_r$  is the difference between PDE already



known and the neural network approximation, where the differential operators are regularly constructed by the Automatic Differentiation [25] to get differential in PDE. Fortunately, the package such Tensorflow and Pytorch [26] have the , function inherently and conveniently, so it is convenient to construct the  $Loss_b$  related to the PDE. The whole Loss function reads as

$$Loss = \frac{\lambda_r}{N_r} \sum_{i=1}^{N_r} |Lu(x_i; \theta)|^2 + \frac{\lambda_b}{N_b} \sum_{i=1}^{N_b} |u(x_i; \theta) - \bar{u}(x_i)|^2 \quad (3)$$

where  $u(x; \theta)$  is the prediction of the coordinate point  $x$  with the neural network parameters  $\theta$ .  $x$  is the coordinate(spatial and temporal) as the input of the neural network, and  $\theta$  is the neural network parameter obtained by the optimization of the loss function.  $L$  is the differential operator, which can be the linear or non-linear differential operator.  $Lu(x; \theta)$  is the PDE equation using the neural network as the interesting field  $u$ .  $\bar{u}(x)$  is the boundary or initial condition data known in advance.  $N_r$  and  $N_b$  are the number of the residual points and the boundary data points respectively.  $\lambda_r$  and  $\lambda_b$  represent the corresponding weight of the residual loss  $Loss_r$  and the boundary loss  $Loss_b$  respectively

$$\begin{aligned} Loss_r &= \frac{1}{N_r} \sum_{i=1}^{N_r} |Lu(x_i; \theta)|^2 \\ Loss_b &= \frac{1}{N_b} \sum_{i=1}^{N_b} |u(x_i; \theta) - \bar{u}(x_i)|^2 \end{aligned} \quad (4)$$

### 2.3. Introduction to DEM

In this section, we introduce the variational principle firstly. Then we explain how to combine the PINN with the principle of minimum potential energy.

If PDE has the variational formulation, the solution of the strong form is equal to the variational formulation, i.e., the solution  $u$  of strong form makes the  $J(u)$  stationary with respect to the arbitrary changes  $\delta u$  [4], where  $J(u)$  represent the functional and  $u$  is a trial function satisfying the essential boundary condition. If neural network loss is the functional, we can get the solution of the strong form by optimization the loss

$$Loss = J(u) \quad (5)$$

$$u^{strong}(x; \theta) = \min_{\theta} J(u(x; \theta)) \approx \min_u J(u) \quad (6)$$

where  $u^{pinn}$  is the solution of the PINN. Although the function space of the neural network is big, there also may be the approximation error, i.e., the error between the true function space and the PINN function space depending on the neural network configuration.  $\theta$  is the neural network parameter. It is worth noting that  $u$  must satisfy the essential boundary condition, i.e., Dirichlet boundary condition.

**Remark 1.** *If the differential operator is linear and self-adjoint, and the highest differential operator order is even. The strong form must have the corresponding minimum potential energy formulation, i.e., the energy formulation is an extreme value problem [4]. In other words, all strong forms have the corresponding weak form, but only the symmetries problem have the corresponding minimum potential energy formulation.*

**Remark 2.** *the trial function  $u$  must satisfy the essential boundary condition, i.e., admissible function*

$$u(x) = \bar{u}(x), x \subseteq \Gamma^u \quad (7)$$

where  $\Gamma^u$  is the essential boundary, and  $\bar{u}(x)$  is the given essential boundary value. In addition,  $u(x) \in H^m$ , if the differential operator is  $2m$  order.  $H$  is the Sobolev space,  $H^m$  means the square of the  $m$ -th derivative of  $u$  is integrable.

### 3. Method

#### 3.1. construction of the admissible function

We can use the penalty method to satisfy the essential boundary condition softly, but the additional hyper-parameter called the penalty factor has to be considered. The most critical challenge of the penalty method is we don't know the best penalty accurately in advance. Therefore, it is necessary to construct the admissible function

$$u(x) = u_p(x; \theta_p) + RBF(x) * u_g(x; \theta_g) \quad (8)$$

where  $u_p(x; \theta_p)$  called particular network is a commonly shallow network trained on the essential boundary to minimize the following MSE loss

$$loss_p = \frac{1}{n_{be}} \sum_{i=1}^{n_{be}} (u_p(x_i; \theta_p) - \bar{u}(x_i))^2. \quad (9)$$

$n_{be}$  is the number of the essential boundary points.

$RBF(x)$  called distance network is a radial basis function to give the nearest distance from  $x \in \Omega$  to  $\Gamma^u$ , where  $\Omega$  denotes the domain of interest field. The number of RBF distribution points and the arrangement need to be determined according to the geometric shape of the essential boundary. In this article, we adopt the commonly used Gaussian function as the basis function

$$RBF(\mathbf{x}) = \sum_{i=1}^n w_i \phi(|\mathbf{x} - \mathbf{x}_i|) \quad (10)$$

where  $w_i$  is the weight of the center  $x_i$  in RBF. The value of  $w_i$  can be obtained according to the training set  $\{x_i, y_i\}$ ,  $y_i$  is the label of  $x_i$ , which is the nearest distance to the essential boundary.  $x$  is the coordinate to be evaluated. We can write the following linear equations to determine  $w_i$

$$\begin{bmatrix} \phi(|x_1 - x_1|) & \phi(|x_1 - x_2|) & \cdots & \phi(|x_1 - x_n|) \\ \phi(|x_2 - x_1|) & \phi(|x_2 - x_2|) & & \vdots \\ \vdots & & \ddots & \phi(|x_{n-1} - x_n|) \\ \phi(|x_n - x_1|) & \cdots & \phi(|x_n - x_{n-1}|) & \phi(|x_n - x_n|) \end{bmatrix} \begin{bmatrix} w_1 \\ w_2 \\ \vdots \\ w_n \end{bmatrix} = \begin{bmatrix} y_1 \\ y_2 \\ \vdots \\ y_n \end{bmatrix} \quad (11)$$

where  $\phi(|\mathbf{x} - \mathbf{x}_i|)$  is named after the radial basis function. Since this function is completely determined by the distance between  $x$  and  $x_i$  regardless of the direction from  $x$  to  $x_i$ , that is the reason called radial. The basis function here is the Gaussian kernel function

$$\phi(r) = \exp(-\gamma r^2) \quad (12)$$

In this article, we adopt  $\gamma = 0.5$ , and we take the same number of fitting points  $\{x_i, y_i\}$  and RBF center points. The number of center points commonly often does not need to take much to construct the distance network, as shown in the later numerical experiment. It is not difficult to prove that the radial basis matrix on the LHS of Eq. (11) is invertible if the center point coordinates are different, and it can accurately satisfy the label value  $y_i$  of the fixed point  $x_i$ . The label value  $y_i$  can be obtained in advance using kdtree [3] and other methods. The accuracy can be improved by increasing the RBF center points, but it will increase the amount of calculation.

$u_g(x; \theta_g)$  called general network is the regulator to let the functional  $J(u)$  minimum.  $u_g(x; \theta_g)$  is also a neural network, whose architecture and activation can be determined according to the specific problem. Note that the form of Eq. (8) ensures that  $u(x)$  satisfies the essential boundary condition if the particular and distance network have been trained successfully. We can see the later numerical experiments show it is easy to train the particular and the distance network successfully. It is important that the admissible function can solve the complex boundary problem, which will be mentioned in detail in section Section 4.2.

**Remark 3.** *The parameter of the particular and the distance network, which should be trained before the general network in advance, must be fixed when training the general network. The order of particular and distance network is not matter*

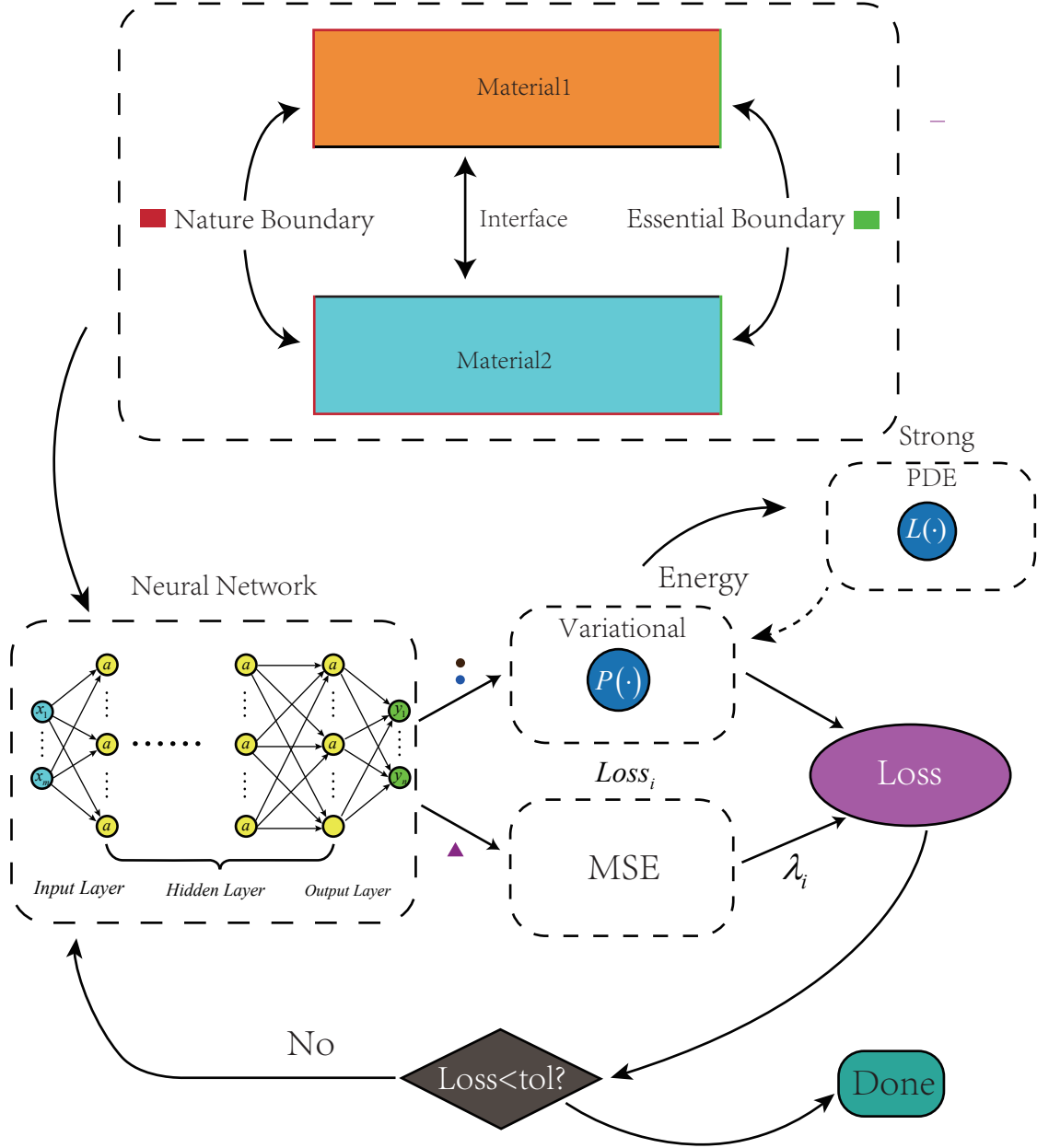


**Fig. 3.** Schematic of CENN : The green line in the upper picture are the essential boundary points, which is used to train the admissible function. The red line in the upper picture is the natural boundary points. The blue and orange region in the upper picture are the domain points corresponding to the different material. The interface points are the black line in the upper picture.  $L(\cdot)$  is the differential operator related to the PDE strong form.  $P(\cdot)$  is the differential operator related to the energy variational form, whose order is lower than the strong form.  $\lambda_i$  is the weight of the interface points.

### 3.2. CENN

In this section, we introduce our proposed method CENN (conservative energy neural network) and the difference with CPINN (Conservative physics-informed neural networks).

Fig. 3 shows the schematic of CENN. CENN is a deep energy method with subdomains and an admissible function. The way to construct the admissible function is illustrated in Section 3.1. The solution is obtained by optimizing the energy function. The energy function adds the additional term called interface loss, which ensures the conservative physic law. For the sake of simplicity, we take the specific PDE equation

$$\begin{aligned}
-a_i \Delta(u(x)) &= 0, x \subseteq \Omega_i \\
u(x) &= \bar{u}(x), x \subseteq \Gamma^u \\
n \cdot a_i(\nabla u(x)) &= \bar{t}(x), x \subseteq \Gamma^{t_i} \\
n \cdot (a^+(\nabla u(x)) - a^-(\nabla u(x))) &= n \cdot (a^-(\nabla u(x))), x \subseteq \Gamma^{inter} \\
u^+(x) &= u^-(x), x \subseteq \Gamma^{inter}
\end{aligned} \tag{13}$$

where  $\Delta$  is the Laplace operator. The interesting field  $u$  is a scalar or tensor, for the sake of simplicity, we consider  $u$  as a scalar.  $\bar{u}$  is the given value of the essential boundary condition (Dirichlet boundary condition).  $\bar{t}$  is the natural boundary condition (Neumann boundary condition).  $\Omega$ ,  $\Gamma^u$ ,  $\Gamma^t$  and  $\Gamma^{inter}$  is the domain, essential bound, natural boundary and interface respectively.  $a$  is the coefficients of PDE and constant in the different regions. The subscript  $i$  represent the different region.  $n$  is the normal direction of the Neumann boundary and the interface. For the sake of simplicity, we analyze two different regions denoted as  $+$  and  $-$ . The variation form is constructed by an integral Galerkin form

$$\begin{aligned}
&\int_{\Omega^+} -a^+(\Delta u) \delta u dx + \int_{\Omega^-} -a^-(\Delta u) \delta u dx + \\
&\int_{\Gamma^{t+}} (n \cdot a^+(\nabla u) - \bar{t}) \delta u dx + \int_{\Gamma^{t-}} (n \cdot a^-(\nabla u) - \bar{t}) \delta u dx + \\
&\int_{\Gamma^{inter}} n \cdot (a^+(\nabla u) - a^-(\nabla u)) \delta u dx + \int_{\Gamma^{inter}} (u^+ - u^-) \delta u dx = 0
\end{aligned} \tag{14}$$

where  $u$  satisfies the essential boundary in advance. We integrate the Eq. (14) by parts, and we can get the weak form with the interface term

$$\begin{aligned}
&\int_{\Omega^+} a^+(\nabla u) \cdot (\nabla \delta u) dx + \int_{\Omega^-} a^-(\nabla u) \cdot (\nabla \delta u) dx \\
&- \int_{\Gamma^{t+} + \Pi^+} a^+ n \cdot (\nabla u) \delta u dx - \int_{\Gamma^{t-} + \Pi^-} a^- n \cdot (\nabla u) \delta u dx \\
&+ \int_{\Gamma^{t+}} (n \cdot a^+(\nabla u) - \bar{t}) \delta u dx + \int_{\Gamma^{t-}} (n \cdot a^-(\nabla u) - \bar{t}) \delta u dx \\
&+ \int_{\Gamma^{inter}} n \cdot (a^+(\nabla u) - a^-(\nabla u)) \delta u dx + \int_{\Gamma^{inter}} (u^+ - u^-) \delta u dx = 0
\end{aligned} \tag{15}$$

where  $\Omega^+$  and  $\Omega^-$  are the different regions of the interesting field.  $\Gamma^+$  and  $\Gamma^-$  are Newmann boundaries of the different region without the interface.  $\Pi^+$  and  $\Pi^-$  are the interface  $\Gamma^{inter}$  of the different region, overlapping each other, and  $n$  is the normal direction of the region  $\Omega^+$  on the interface, i.e.,  $n = n^+ = -n^-$ . We combine the similar items

$$\begin{aligned}
&\int_{\Omega^+} a^+(\nabla u) \cdot (\nabla \delta u) dx + \int_{\Omega^-} a^-(\nabla u) \cdot (\nabla \delta u) dx \\
&- \int_{\Gamma^{t+}} \bar{t} \delta u dx - \int_{\Gamma^{t-}} \bar{t} \delta u dx + \int_{\Gamma^{inter}} (u^+ - u^-) \delta u dx = 0.
\end{aligned} \tag{16}$$

The Eq. (16) is equal to the energy stationary, so we can get the energy form with the interface,

$$J = \frac{1}{2} \int_{\Omega^+} a^+ (\nabla u) \cdot (\nabla u) dx + \frac{1}{2} \int_{\Omega^-} a^- (\nabla u) \cdot (\nabla u) dx - \int_{\Gamma^{t+}} \bar{t} u dx - \int_{\Gamma^{t-}} \bar{t} u dx + MSE(u^+ - u^-)|_{interface} \quad (17)$$

Further, the above energy form is a convex function, and the true solution is the stationary point, i.e., the extreme value problem. It is worth noting that although the energy form is convex in terms of the whole function space, it is commonly not convex in the neural network function space. So we can get the solution by optimizing  $J$  to a minimum. We can assign the different neural network in each subdomain. The backpropagation of CENN is discussed in Appendix B. CENN penalty only has one unknown penalty on the interface to ensure the continuity of the interesting field. However, CPINN not only has the  $u$  continuity condition but also has the derivative of  $u$  continuity condition. The additional derivative of CPINN will decrease the accuracy and efficiency. If the order of the PDE increase, the additional term about interface will increase in CPINN more than CENN, e.g., if the order of PDE is  $2m$  order derivative, it is easy to prove that CPINN will have  $m$  more interface penalty factors than CENN. However, there is no way to determine the CPINN penalty factor, i.e., the different components of the loss function, to the best of my knowledge. Compared with CPINN, the penalty of CENN is greatly reduced, but still, there is a penalty of the interface, which is a hyperparameter. Here we use a heuristic construction

$$\beta = -c * \ln(\tanh(\frac{N_{interface}}{N_{domain}})) \quad (18)$$

where  $\beta$  is the hyperparameter of the interface, and  $c$  is a scale factor, we recommend  $1e3$ .  $N_{interface}$  and  $N_{domain}$  are the number of points at the interface and the domain, respectively. The above formula uses the concept of information entropy, we assume that  $p = \tanh(N_{interface}/N_{domain})$  is the probability of the certainty of the interface. Obviously, the more interface points, the greater certainty of probability about the interface. Because the training is essentially a multi-task learning, it is a game between the interface loss and the energy functional. If there are more interface points, the attention to the training of the energy functional is less. We need to adjust the hyperparameter  $\beta$  to balance the interface loss and energy loss. Finally,  $-\ln(p)$  is the information entropy to evaluate the value of the interface information, i.e., it indicates that the interface has more abundant information if there are more interface points. The above heuristic construction is used to construct the penalty of the interface. After many numerical experiments, we found that training is successful by this construction of the hyperparameter.

**Remark 4.** CENN is suitable for solving the problem of one point coordinate containing multiple values of interesting field, such as the crack problem, which will be mentioned in detail in section Section 4.1. CENN is also suitable for solving the problem of weak continuity problem, i.e., the problem that the original function is continuous but the derivative function is discontinuous, such as heterogeneous problem, which will be mentioned in detail in Section 4.2 and Section 4.3.

## 4. Result

### 4.1. Crack

The governing equation of III mode crack is given by

$$\Delta(u(x)) = 0, x \in \Omega \quad (19)$$

where  $\Omega = (-1, 1) \times (-1, 1)$ . The analytical displacement solution is  $u = r^{\frac{1}{2}} \sin(\frac{1}{2}\theta)$ ,  $r$  and  $\theta$  are the radius and the angle of polar coordinates, and the  $\theta$  range is  $[-\pi, +\pi]$ . We construct the boundary conditions through the analytical solution. It is worth noting that the solution to this problem suffers from the well-known ‘‘corner singularity’’, which means that the derivative is one-half singularity at the center point(0, 0) [4]. Because the displacement solution of this problem is discontinuous at the crack( $x < 0, y = 0$ ), the same coordinate point at

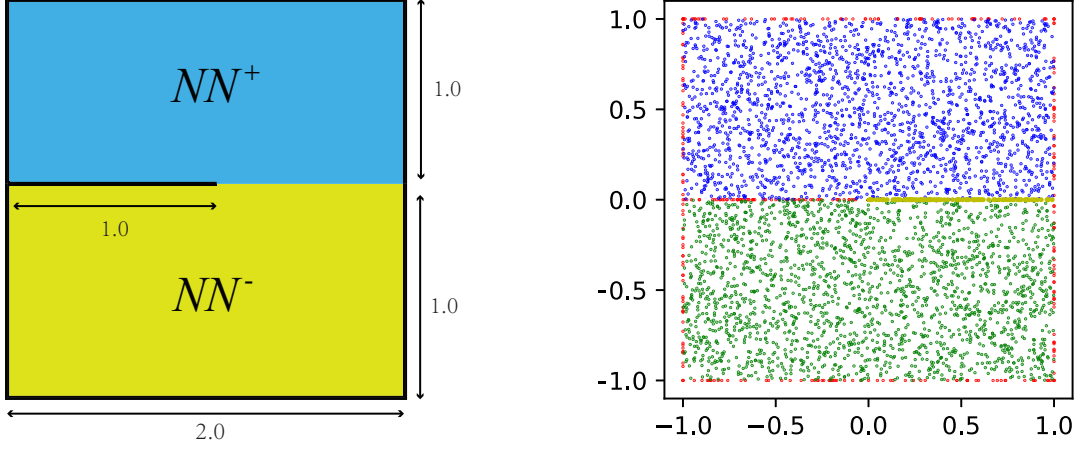


**Fig. 4.** The schematic diagram of III mode crack:  $NN^+$  represents the neural network in the upper area,  $NN^-$  represents the different neural network in the lower area, the geometric size is a square with side length 2, the length of the crack is 1, spanning in the middle of the structure, i.e.,  $x < 0, y = 0$  (left). Illustration of different sampling sizes and strategies, the blue points are the internal training points of the neural network  $NN^+$ , the green points are the internal training points of the neural network  $NN^-$ , the red points are the training points of the essential boundary conditions, and the yellow points are the interface points of the different neural network, the total number of internal points in the upper and lower regions is 4096, the number of essential boundaries condition points is 256, and the number of interface points is 1000. All points are randomly distributed unless otherwise stated (Right).

the crack corresponds to multiple displacement values  $\pm r^{\frac{1}{2}}$ , so it is necessary to use two neural networks to approximate the displacement field. We divide the area into upper and lower parts, and use different neural networks to approximate them, as shown in Fig. 10 (left), considering the current commonly used method: data-driven and CPINN, so we compare data-driven, CPINN (PINN strong form with subdomains) and CENN (deep energy form with subdomains), the above three methods have the same point allocation way, as shown in Fig. 10 (right). Training points are redistributed every 100 epochs in all three methods. The energy principle needs to convert the above strong form into a variational form. The variational form of the Eq. (19) is

$$J(u) = \int_{\Omega} \frac{1}{2} (\nabla u) \cdot (\nabla u) d\Omega. \quad (20)$$

Using the energy principle, the minimum value of the above formula is equivalent to the strong form of the solution, but the energy principle needs to construct a possible displacement field, i.e., the admissible function. It is necessary to find a certain displacement in the possible displacement field, so that the functional Eq. (20) takes the minimum value, and the displacement is considered to be the optimal solution in the sense of optimal energy error, i.e.,  $\int_{\Omega} Energy(u^* - u^{pred}) d\Omega$ , where  $u^*$  and  $u^{pred}$  is the exact value and prediction of the problem [4].

Therefore, compared with the strong form, CENN requires additional construction of possible displacement fields that meet the essential boundary conditions. The RBF distance network and the particular network that meets the essential boundary conditions need to be constructed in advance. The number of RBF allocation points and the arrangement of points need to be determined according to the geometric shape of the essential boundary conditions. Here, there are 45 points on the boundary and 7 points in the domain as shown in Fig. 5 (left). RBF distance network prediction is shown in Fig. 5 (right). The average error of the RBF network is about 0.37 %. The accuracy can be improved by increasing the RBF center point including boundary points and the domain points, but it will increase the amount of calculation. After obtaining the RBF distance network, we train two particular networks in the upper and lower region to fit the essential boundary conditions. The hidden layer of the particular network has 3 layers, each layer has 10 neurons more shallow than the general network, the activation function is tanh in all hidden layers, and an identical function is used in the output layer, the optimizer is Adam [27], the learning rate is  $5e-4$ . It is worth noting that the neural network structure

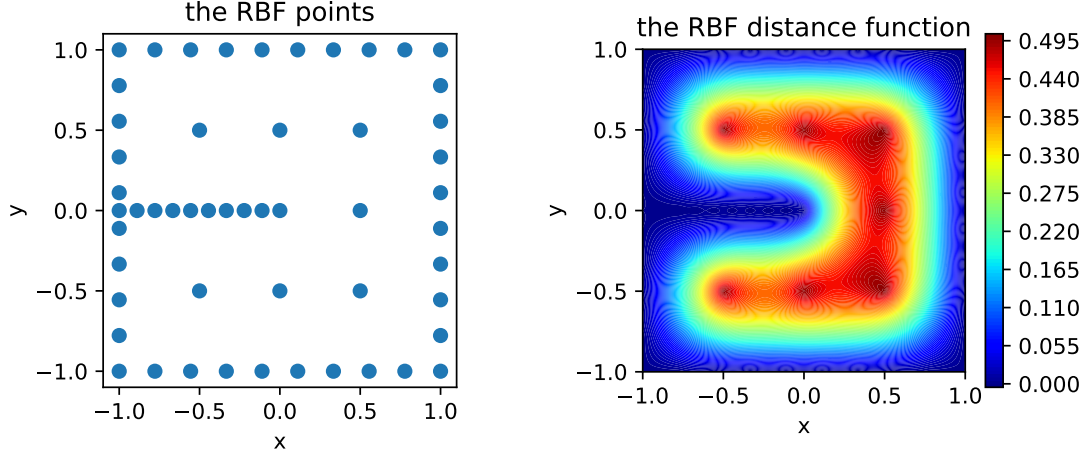


**Fig. 5.** The RBF distance network of III mode of the crack: RBF points allocation map (left), RBF distance network prediction contour (right)

of the particular solution network does not need to be too complicated thanks to the powerful fitting ability of the neural network. A simple neural network structure can fit the essential boundary conditions well. It is worth noting that we must add  $Loss_{interface} = ||u^+ - u^-||$  at the interface to satisfy the continuity, and the convergence condition of the particular network training is that the MSE is less than  $1e-6$ . Fig. 6 (upper left and mid) shows the output of the particular network is close to the pattern of the exact solution because the boundary conditions are all essential boundary conditions enclosing the interesting domain. As shown in Fig. 6 (upper right), the network structure can fit the boundary value well as the number of network training rounds increases. The loss function of the boundary drops a little faster than the loss value of the interface because there is a specific label at the boundary. However, the loss at the interface is the difference between different neural networks. It is a soft constraint easily affected at the interface. The convergence speed of the boundary loss of different particular networks is almost the same, which shows that the particular network can learn the x-axis center symmetry of the exact solution very well. It does not matter the particular network and the exact solution are quite different in the domain without essential boundaries. Because the function of the particular network is to precisely satisfy the given value at the essential boundary conditions. To further explore the performance of the particular network, we make a clockwise circle around the essential boundary as shown in Fig. 6 (lower left). Fig. 6 (lower right) shows the comparison of the particular network and the exact solution at the essential boundary. We can find that the particular network can fit the essential boundary conditions very well, which comes from the powerful fitting ability of the neural network.

After constructing the possible displacement field, we compare data-driven, CPINN and CENN. The number of allocation points of these three ways is the same. The network structure and optimization scheme are also the same. It is worth noting that CPINN does not use the construction of the admissible function, but the other two methods (data-driven and CENN) use that. Here the structure of the generalized network is 4 layers, each layer has 20 neurons, and the learning rate is 0.001. We consider the admissible function

$$u(x) = u_p(x; \theta_p) + RBF(x) * u_g(x; \theta_g) \quad (21)$$

where  $u_p$  is the particular network,  $\theta_p$  is the parameter of the particular network, RBF is the radial basis function,  $u_g$  is the generalized network,  $\theta_g$  is the parameter of the generalized network. In the training process, we freeze the parameters of the particular network and RBF, and only train the generalized neural network through the gradient descent method, i.e., Adam. It is worth noting that RBF is equal to zero at the essential boundary, so the role of the generalized network is eliminated, which results that the particular network only plays games. If the training of the RBF and particular network is successful, the admissible function accurately meets the given displacement value at the essential boundary, which is the heart of the admissible function.



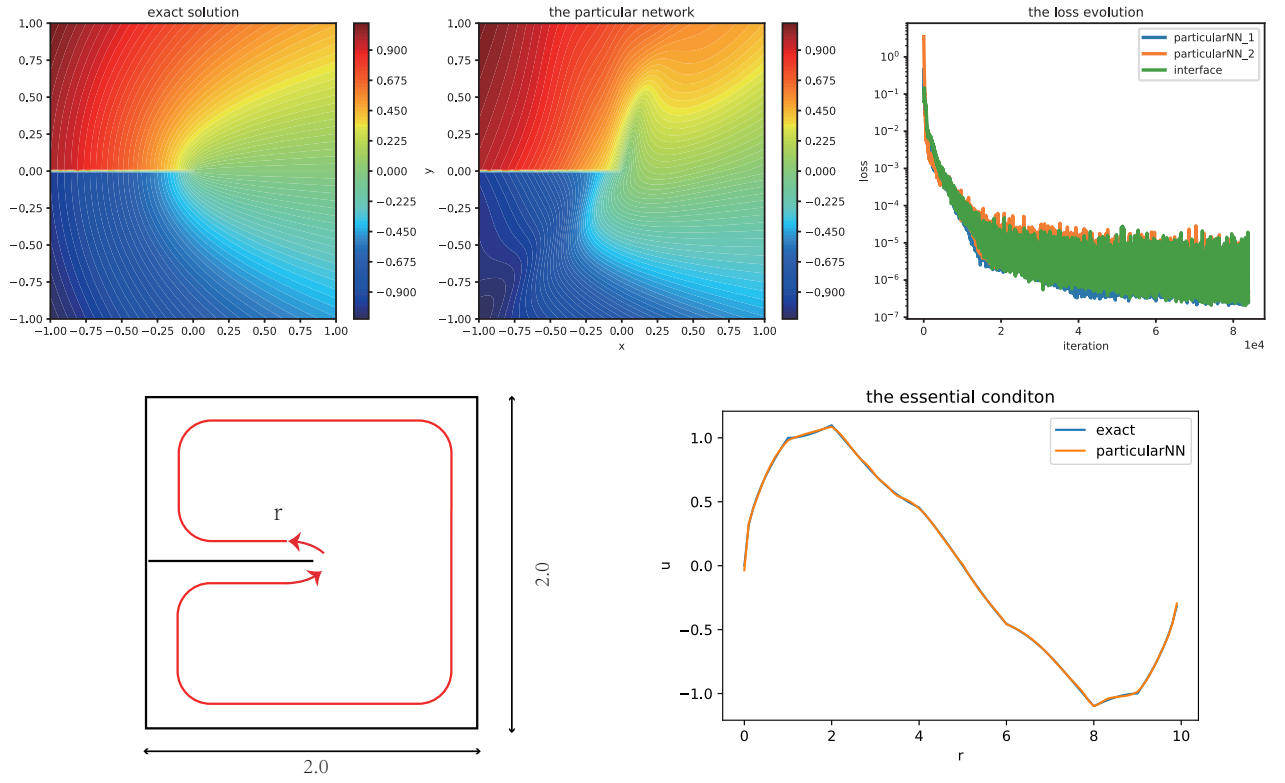


**Fig. 6.** The contour of the exact solution of III mode crack (upper left). The contour of the particular prediction (upper mid). Evolution of the MSE loss for the training particular network, particular\_1 and 2 represents the evolution of the different particular network loss, the number and the arrangement of points in both neural networks are same, points are redistributed every 10 epoch (upper right). The evaluation trace of the particular solution, starting from the center point and going around the boundary clockwise (down left). The comparison of the particular network and the exact solution on the trace of the boundary clockwise (down right)

On the other hand, the CPINN subdomains are the same as CENN, i.e., the upper and lower neural networks. The boundary conditions and the interface conditions are imposed by the penalty method, noting that the interface conditions include not only the continuous condition of displacement but also the continuous condition of displacement derivative, i.e.,

$$\begin{aligned} n \cdot (\nabla u^+ - \nabla u^-) &= 0, x \in \Gamma^{inter} \\ u^+(x) &= u^-(x), x \in \Gamma^{inter}. \end{aligned} \quad (22)$$

Compared to CENN, one more loss is added, and the additional loss function is the derivative form, which will reduce the accuracy and efficiency. The loss function of CPINN is

$$\begin{aligned} Loss &= \lambda_1 \int_{\Omega^+} |\Delta(u^+)|^2 d\Omega + \lambda_2 \int_{\Omega^-} |\Delta(u^-)|^2 d\Omega + \lambda_3 \int_{\Gamma^+} |u^+ - \bar{u}|^2 d\Gamma + \lambda_4 \int_{\Gamma^-} |u^- - \bar{u}|^2 d\Gamma \\ &+ \lambda_5 \int_{interface} |u^- - u^+|^2 d\Gamma + \lambda_6 \int_{interface} |n \cdot (\nabla u^+ - \nabla u^-)|^2 d\Gamma \end{aligned} \quad (23)$$

It is not difficult to find that there are many hyperparameters in CPINN (more subdomains will further increase hyperparameters). Through tuning repeatedly, we have selected the best set of hyperparameters,  $\lambda_1 = \lambda_2 = 1, \lambda_3 = \lambda_4 = 50, \lambda_5 = \lambda_6 = 10$  (maybe there are better hyperparameters, because there are 6 hyperparameters, the workload of tuning parameters is very large). Some articles show that it is possible to use NTK theory to automatically adjust hyperparameters for PINN [22], but there is no method for hyperparameter adjustments in the form of subdomain PINN, i.e., CPINN. Fig. 7 (left) shows the data-driven prediction results and absolute error, Fig. 8 (right) shows that the overall relative error of the data-driven is 1.55 %. Due to the randomness of the initial parameters of the neural network, the initial parameters are initialized with Xavier [28], i.e. a method to initialize parameters, if not specified, all the results below are the average of 5 times. Since data-driven does not consider PDE, the loss function does not include auto differential [25], which has higher accuracy and computational efficiency. We found the absolute error near the center ( $x=0, y=0$ ) is the largest as shown in Fig. 7 (lower left). Fig. 9 (first row) shows that the exact solution is not smooth at the center. This may be the reason for the large error at the center point. In addition, there were relatively sharp fluctuations at the beginning loss evolution, and then gradually converged. Fig. 7 (middle) shows that the prediction results of CPINN are sharp relatively, and the errors are also mainly concentrated in the center point. Because the derivative of analytical solution with respect to  $\theta$  is singular at the center point, causing the loss at the center point to fluctuate sharply. Considering that CPINN and data-driven are both MSE errors, the optimal loss values both are 0, so we compare the loss functions of the two together as shown in Fig. 8 (left). In addition, CENN is based on the energy method, and the loss function is an energy functional, so the optimal loss value is not 0. From Fig. 8 (left), it can be seen that the CPINN loss function is higher than data-driven. The CPINN loss function is unstable compared to the data-driven, which is due to the high-order derivatives involved. In addition, the decreasing trend of the loss function of the different networks is similar in CPINN. This is because the problem is about the x-axis symmetry. To further analyze the performance of these three methods, we compare the relative error  $L_2 = \sqrt{\sum_{i=1}^{N_{pred}} error^2(x_i)} / \sqrt{\sum_{i=1}^{N_{pred}} exact^2(x_i)}$ . Fig. 8 (right) shows that the overall relative error of CPINN is 5.04 %. This may be one of the reasons that the weight of the different loss functions is not adjusted to the optimal value. In addition, CPINN involves higher-order derivatives, so the efficiency and accuracy are not as good as CENN. Fig. 7 (right) shows that the prediction result of CENN is smooth, not as sharp as CPINN. Fig. 8 (right) shows that the overall relative error of CENN is 1.42 % and the overall result is better than CPINN and even better than data-driven accuracy. Due to the low derivative order of the loss function, the efficiency is higher than CPINN. The error distribution is more uniform. The main error is at the center point ( $x=0, y=0$ ), which is caused by the form of the admissible function. This will be analyzed in the discussion part Section 5 in detail. Fig. 8 (middle) shows that the trend of the CENN loss function converges to the exact value of the functional

$$J = \int \frac{1}{2} \left[ \left( \frac{\partial u}{\partial r} \right)^2 + \left( \frac{\partial u}{r \partial \theta} \right)^2 \right] r dr d\theta = \int \left[ \frac{1}{8\sqrt{x^2 + y^2}} \right] dx dy.$$

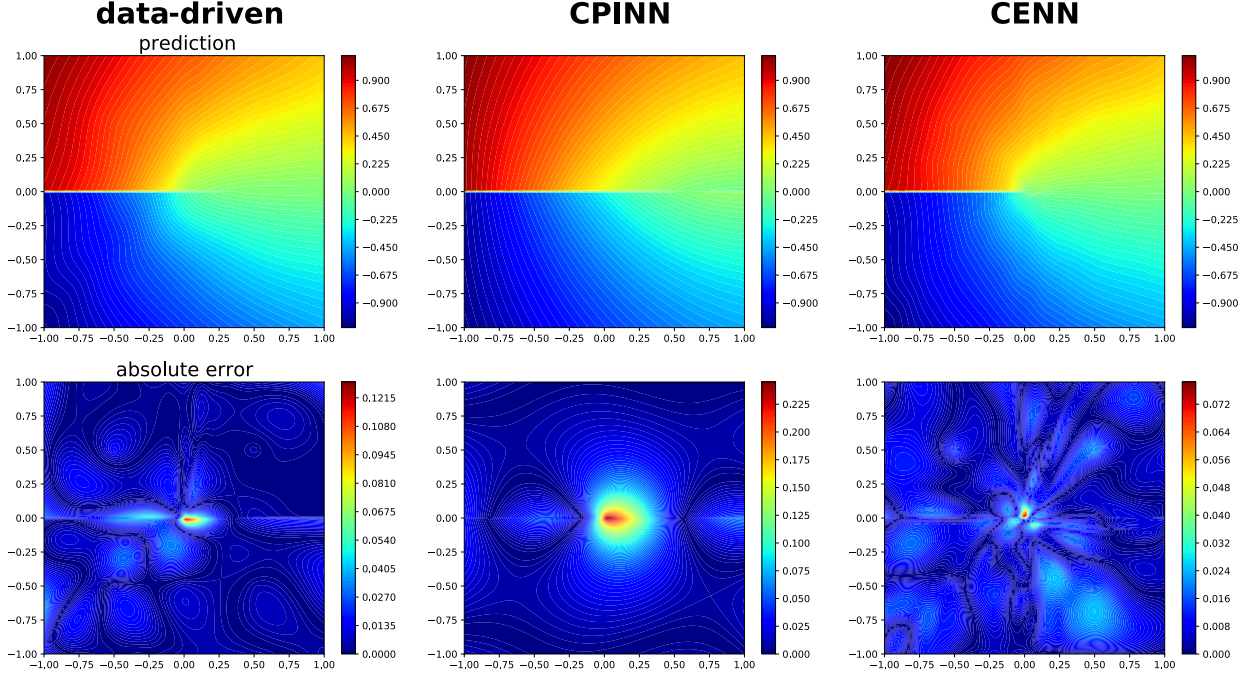


**Fig. 7.** Predicted solution and absolute error by data-driven, CPINN and CENN in III mode crack: The displacement field prediction result (first row), absolute error (second row).

The analytic integral of the analytic energy functional is about 0.8814. According to the principle of minimum potential energy, the real solution is the minimum value of the energy functional, i.e., 0.8814 in this problem. The reason for a small amount of fluctuation in the later stage of the training is due to the learning rate. This can be eliminated by reducing the learning rate. In addition, the loss function is sometimes slightly lower than the exact value due to numerical integration and discrete errors, which can be reduced by increasing random points. Fig. 8 (right) shows that CENN surpasses CPINN obviously, and even surpasses data-driven not involving coordinate derivatives. Finally, we can find that the trends of the loss function and relative error of the above three methods are the same.

Next, we compare the discontinuous displacement solutions and singular strains that we are more concerned about. Fig. 9 show the comparison of solution of data-driven, CPINN and CENN at various  $x$  and  $y$  position. We observe the displacement of  $y=0$ , the up and down displacement. This is because at  $(x<0, y=0)$ , the displacement solution is multiple values of the same coordinate, so there are two displacement solutions as shown in Fig. 9 (upper). We take into account the strain

$$\varepsilon_{z\theta}|_{interface} = \frac{1}{r} \frac{\partial u}{\partial \theta} = \frac{1}{2\sqrt{r}} \cos\left(\frac{\theta}{2}\right)|_{\theta=0} = \frac{1}{2\sqrt{r}}, \quad (24)$$

the  $y$ -direction derivative of the displacement is singular at the center  $(x=0, y=0)$ , so we research the singular strain at the interface, and explore whether the neural network is capable of fitting the singularity problem. Fig. 9 (up) shows that the prediction of CENN and data-driven is close to the displacement solution, and both have higher accuracy than CPINN. The error between CENN and data-driven is large at  $x=0$ , which is caused by the RBF distance network of the admissible function, which will be further analyzed in Section 5. Fig. 9 (down left) shows the comparison of  $x=0$ . The accuracy of CENN at  $x=0$  is higher than that of data-driven as the same as  $y=0$ , and the error near the center point is higher. It is also the reason that the RBF distance network of the admissible function causes. Fig. 9 (down right) shows the singular strain. The performance of CENN in singular strain is much stronger than data-driven and CPINN. This is because loss function of CENN is constructed based on the physical minimum energy theory whose interpretability is stronger. The

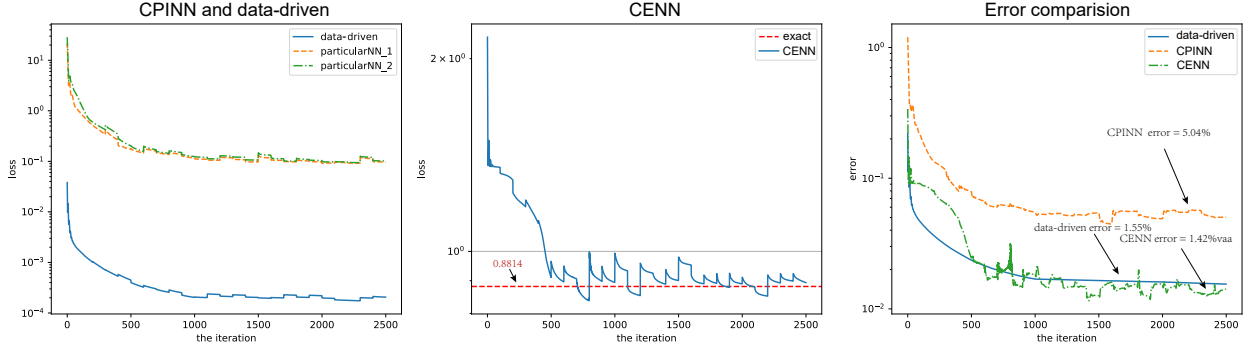


**Fig. 8.** Comparison the loss and error of data-driven, CPINN and CENN in III mode crack: Comparison of the loss function of CPINN and data-driven (left), comparison of the CENN loss function with precise functional integral (middle), comparison of the overall relative error of data driven, CPINN and CENN (right)

strain will cause the loss function to change in CENN, which will make the CENN strain converge to the exact solution. In numerical methods such as finite element, the singular point of fracture mechanics often requires a special quarter-node element [4], but this method does not have a special treatment, which comes from the huge function space of the neural network itself.

**Remark 5.** DEM is a special form of the weighted residual. The test function of DEM is  $\frac{\partial u(x;\theta)}{\partial \theta_j}$ , the test function of traditional PINN is  $2\Delta \frac{\partial u}{\partial \theta_j}$ . Due to the huge function space of test and trial function, DEM and PINN can successfully approximate the solution of the PDE to some extent.

**Proof.** The proof can be found in [Appendix A](#) □

#### 4.2. Non homogeneous problem with the complex boundary

In this section, we consider the problem with the complex boundary, which can not be solved well in a traditional method such as FEM [3]. So we consider the Koch snowflake as our boundary. We also consider the non-homogeneous problem, which is widespread in physics such as composites material, as shown in [Fig. 10](#) (left), the fractal level  $L=2$ . The farthest point of the Koch snowflake from the center is 1.5. The govern equation of the problem is [18]

$$\begin{cases} -a(x)\Delta u(x) = f(x) & x \in \Omega \\ u(x) = g(x) & x \in \partial\Omega \end{cases} \quad (25)$$

where  $\alpha(x) = \alpha_i, x \in V_i$ ,  $\alpha$  for different regions is a different constant. For sake of simplicity, we consider

$$\begin{cases} a_1 = \frac{1}{15} & r < r_0 \\ a_2 = 1 & r \geq r_0 \end{cases} \quad (26)$$

We adopt the exact solution

$$u(r, \theta) = \begin{cases} \frac{r^4}{\alpha_1} & r < r_0 \\ \frac{r^4}{\alpha_2} + r_0^4 \left( \frac{1}{\alpha_1} - \frac{1}{\alpha_2} \right) & r \geq r_0 \end{cases} \quad (27)$$

The energy form of the problem is

$$J = \int_{\Omega_1} \frac{1}{2} \alpha_i (\nabla u) \cdot (\nabla u) d\Omega + \int_{\Omega_2} \frac{1}{2} \alpha_i (\nabla u) \cdot (\nabla u) d\Omega - \int_{\Omega} f u d\Omega \quad (28)$$

where  $\Omega_1$  is the domain  $r < r_0$  and  $\Omega_2$  is the domain  $r \geq r_0$ ,  $r_0 = 0.5$ . It is worth noting that the exact solution is  $C_0$ , but the derivative of  $u$  with respect to  $r$  is discontinuous on the interface.

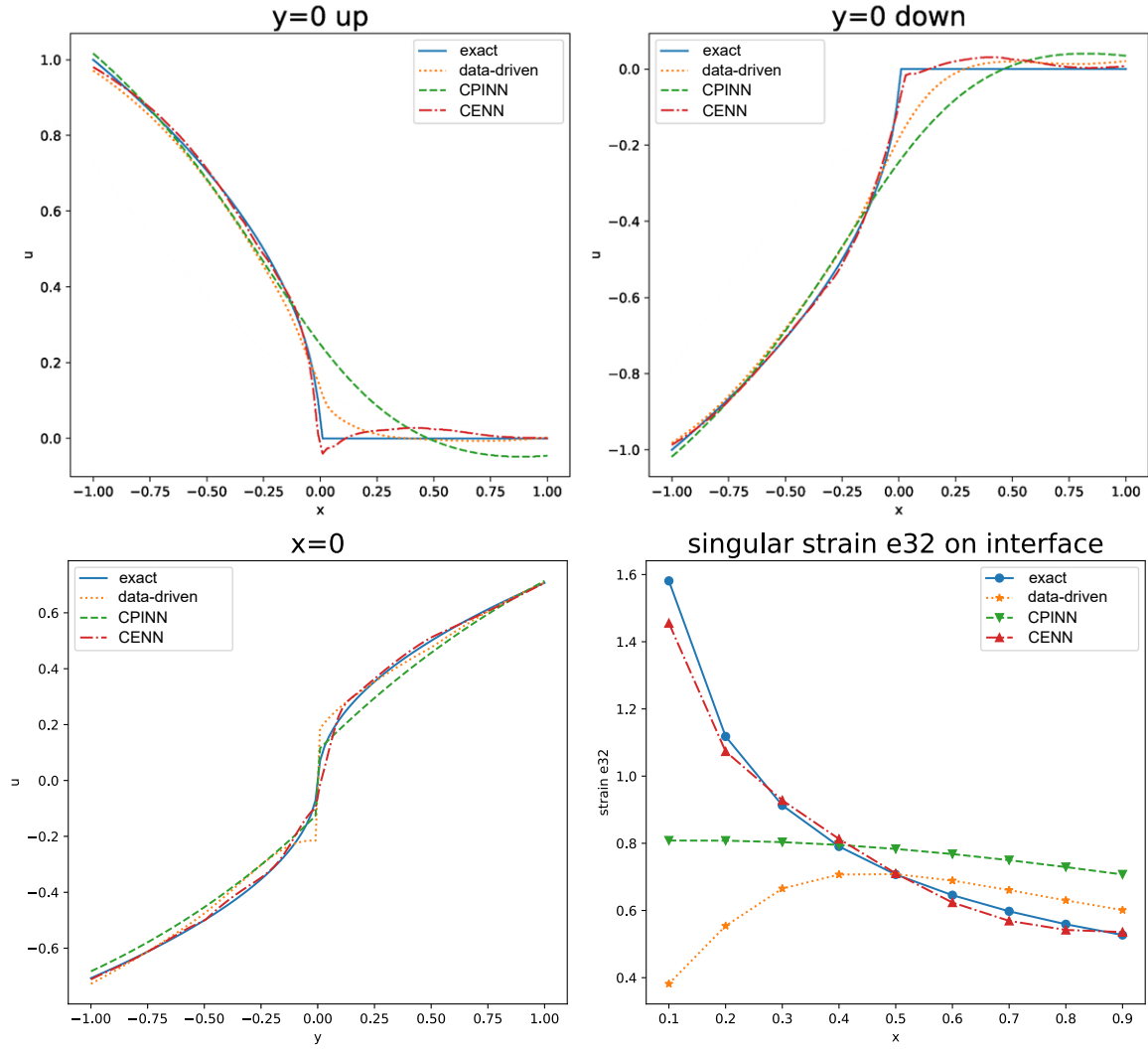


**Fig. 9.** Different location comparison among Data-driven, CPINN, and CENN : Comparison of the displacement solution on the horizontal line  $y=0$  up (upper left), comparison of the displacement solution on the horizontal line  $y=0$  down (upper right), comparison of displacement solution in  $x=0$  (lower left), comparison of displacement derivative  $\frac{\partial u}{\partial y}$  at  $x>0, y=0$  (lower right)

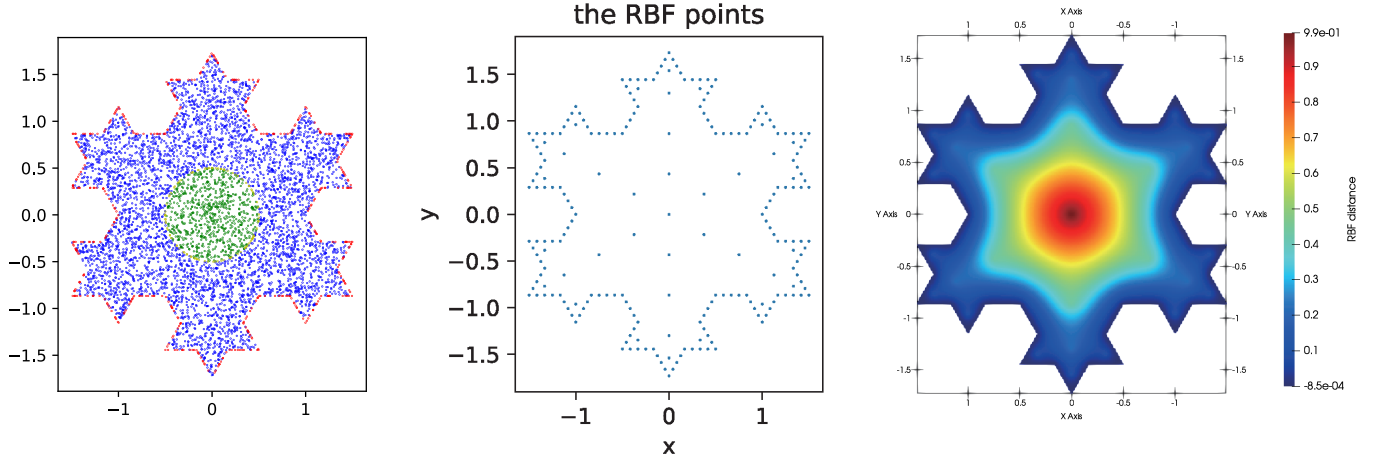


**Fig. 10.** Distance network with complex boundaries of inhomogeneity: Illustration of different sampling size and points allocation strategy, the green points are the  $a = 1/15 (r < 0.5)$  training points, the blue points are the  $a = 1 (r > 0.5)$  training points, the red points are the training points of the essential boundary conditions, and the yellow points are the interface points ( $r = 0.5$ ) of the different domain, the total number of domain points is 10000, the number of essential boundary condition points is 4800, and the number of interface points is 1000. All points are randomly distributed (left). The collocation point diagram of RBF network, 192 points on the boundary, 37 points in the domain (mid), prediction of RBF distance network (right)

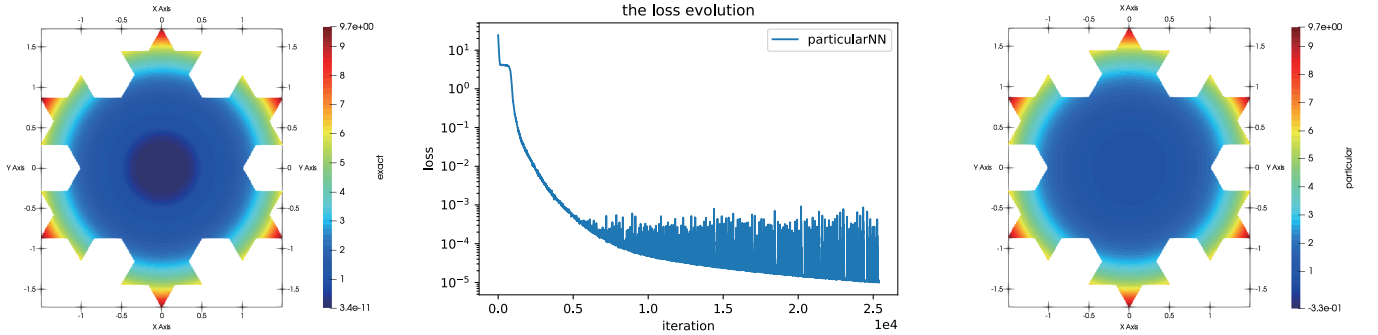


**Fig. 11.** Koch particular neural network : the contour of the exact solution of Koch (left), the evolution of the MSE loss for the training particular network (mid), the contour of the particular prediction (right)

The RBF distance network in the possible displacement field is shown in Fig. 10 (mid and right), which has more collocation points than the crack problem due to the complex boundary conditions. We can find the prediction of the RBF distance network matches the accurate distance.

The convergence condition of the particular network training is that the MSE is less than  $1e-6$ . The hidden layer of the particular network has 4 layers, each layer has 20 neurons, the activation function is tanh in all hidden layers, and an identical function is used in the output layer, the optimizer is adam, the learning rate is  $5e-4$ . Fig. 11 shows the particular pattern is close to the exact solution. The reason is that the essential boundaries enclose the domain. The loss function of the particular neural network decreases as the number of iterations increases, which shows the particular network can fit the essential boundary well. The oscillation of the loss is the reason that the learning rate is not adequate small, we can decrease the learning rate to eliminate the oscillation phenomenon.

Considering that the derivative on the interface is discontinuous, we compare CPINN, DEM, and CENN. We divide the domain into 2 subdomains, using the derivative discontinuity, i.e.,  $r = 0.5$ , as the partition interface. The neural network architecture is the same in the subdomain, which can be also different. The hidden layer of the particular network has 4 layers, each layer has 20 neurons, the activation function is tanh in all hidden layers, and identical function is used in the output layer, the optimizer is adam, the learning rate is  $1e-3$ . The training



points are randomly distributed in all methods as shown in Fig. 10 (left). Training points are redistributed every 100 epochs in all three methods. The penalty  $\lambda$  of every loss function in CPINN :  $\lambda_1 = 60$  when  $r < r_0$ ,  $\lambda_2 = 1$  when  $r > r_0$ ,  $\lambda_{inter}=1$  when  $r = r_0$ ,  $\lambda_{bound} = 30$  on the essential boundary. It is worth noting that the loss on the interface includes

$$\begin{cases} u^+ = u^- \\ a_1(n \cdot \nabla u^+) = a_2(n \cdot \nabla u^-) \end{cases} \quad (29)$$

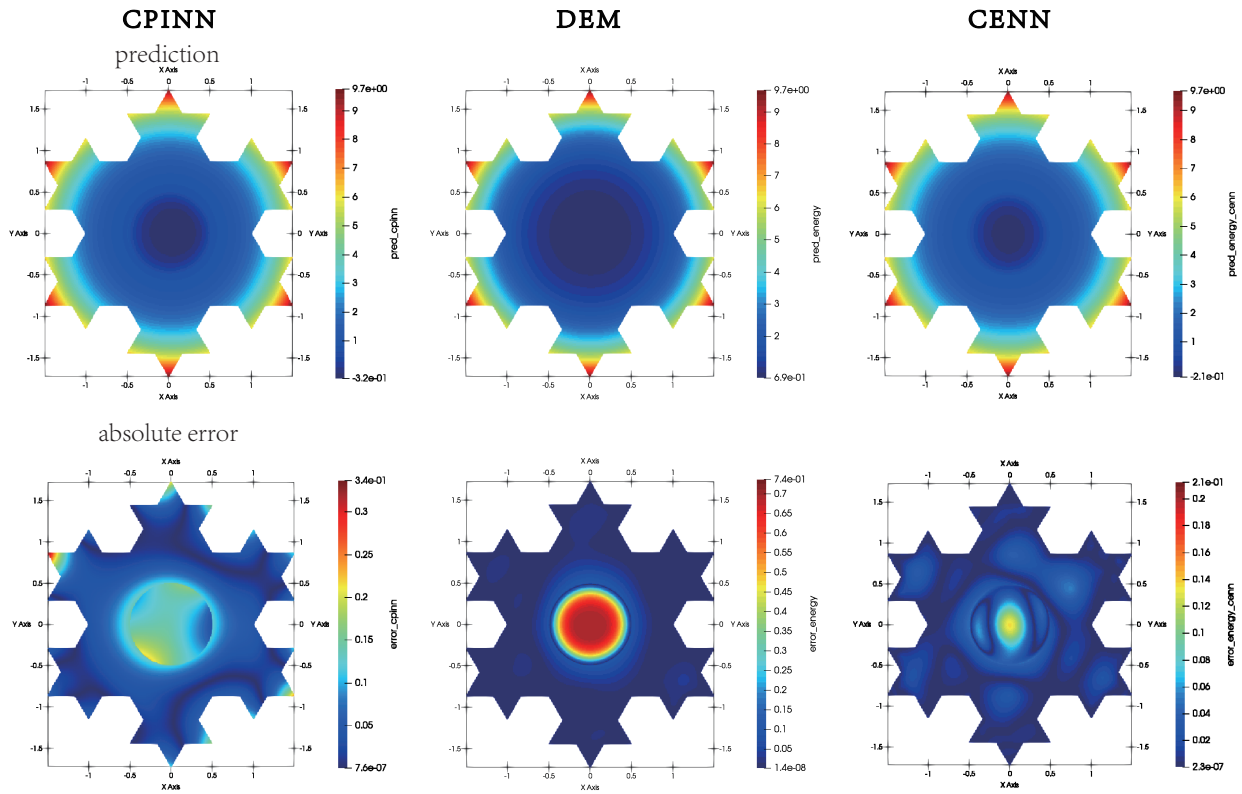
where  $u^+$  and  $u^-$  represent the internal and external region neural network respectively. For sake of simplicity, the two interface loss terms are controlled by the same penalty  $\lambda_{inter}$ . We adopt sequential training for two neural networks [29]. In particular, we first optimize  $u^+$  parameters with  $u^-$  parameters fixed for 20 epochs, then vice versa in CPINN. DEM and CENN are trained by the admissible function. CENN is trained by sequential training to pay attention to the internal energy (internal), given that the difference between the energy of internal and external is too large. we first optimize  $u^+$  parameters with  $u^-$  parameters fixed for 2500 epoch in CENN, then vice versa. We use the admissible function in the external region, while not in the internal region because the whole boundary condition is in the external region. We stitch the subdomains through the interface loss.

Fig. 12 shows the prediction and absolute error of these three methods. The maximum absolute error of CPINN is on the boundary, which may be the reason that the second-order derivation of the solution is big on the boundary in CPINN, resulting in the prediction sensitivity on the boundary. The error of DEM is mainly in the middle of the region ( $r < r_0$ ), because the energy density  $\frac{1}{2}\alpha_1(\nabla u) \cdot (\nabla u) = 8r^6/a_1$  is much smaller than the external energy density. The huge difference in internal and external energies results in paying too much attention to the external region. The maximum absolute error in CENN, CPINN, CENN is 0.34, 0.74, and 0.11 respectively. The error in the CENN is mainly concentrated in the area near the center point, which is obviously smaller than DEM in terms of error magnitude and range. In CENN, It is maybe that the energy density  $\frac{1}{2}\alpha_1(\nabla u) \cdot (\nabla u) = 8r^6/a_1$  is close to zero when  $r$  is close to the center point. So the loss of the internal will pay attention to the region where the loss can be decreased faster, resulting in the error in the center point.

To further analyze the performance of these three methods, we compare the loss and relative error  $L_2$ . Considering that the loss of DEM and CENN are both energy variational, so the optimal values both are the same, so we compare the loss functions of these two methods together as shown in Fig. 13. Due to the complexity of the boundary conditions, we calculate the exact numerical integral for this case by the Monte Carlo algorithm, which is 437. 55, with an exact value of 1. 10 for the internal integral and 436. 45 for the external. For better visualization, we normalize the energy loss. Fig. 13 (upper left) shows the trend of the different part loss evolution in CPINN are similar, which proves our choice of the penalty is relatively good. Fig. 13 (upper right) shows DEM can not converge to the exact internal energy, which is the reason why the absolute error in the internal region is obviously large than the external region. However, CENN can converge to the exact internal energy well due to the subdomains. Fig. 13 (lower left) shows CENN and DEM both converge to the external energy because the external energy dominates the majority of the total energy. The fluctuation in the external and internal energy can be eliminated by decreasing the learning rate. Fig. 13 (lower right) shows the relative error  $L_2$  is 4.9 %, 6.5 %, and 0.7 % in CPINN, DEM, and CENN respectively. Obviously , CENN can solve the composite problem very well, and there is only one hyperparameter penalty about the interface in the loss function. Finally, we can find that the trends of the loss function and relative error of the above three methods are the same.

To further analyze the interface prediction of these three methods, we compare the solution and the discontinuous derivative on the interface. Fig. 14 (upper) shows the comparison of solution of CPINN, DEM and CENN at two cross lines,  $x=0$  and  $y=0$ . CENN prediction about the solution is most accurate among these methods, and the error increases slightly near the center area, the reason may be relatively little energy density in the center point. The center error may be alleviated by adopting more points in the internal region, which we will further study in the future. It is worth noting that the derivative solution by CPINN is more accurate than CENN and energy method, as shown in Fig. 14 (lower). The reason may be the second-order derivative used in CPINN is not smaller than the first-order derivative in CENN in the internal region, so the derivative in the internal region can be trained well by strong form. It is worth noting the solution prediction of these three methods is smaller than the exact solution, which is suitable for some engineering conservative problems.





**Fig. 12.** Prediction and absolute error by CPINN, DEM, and CENN in Koch: The displacement field prediction result (first row), absolute error (second row).

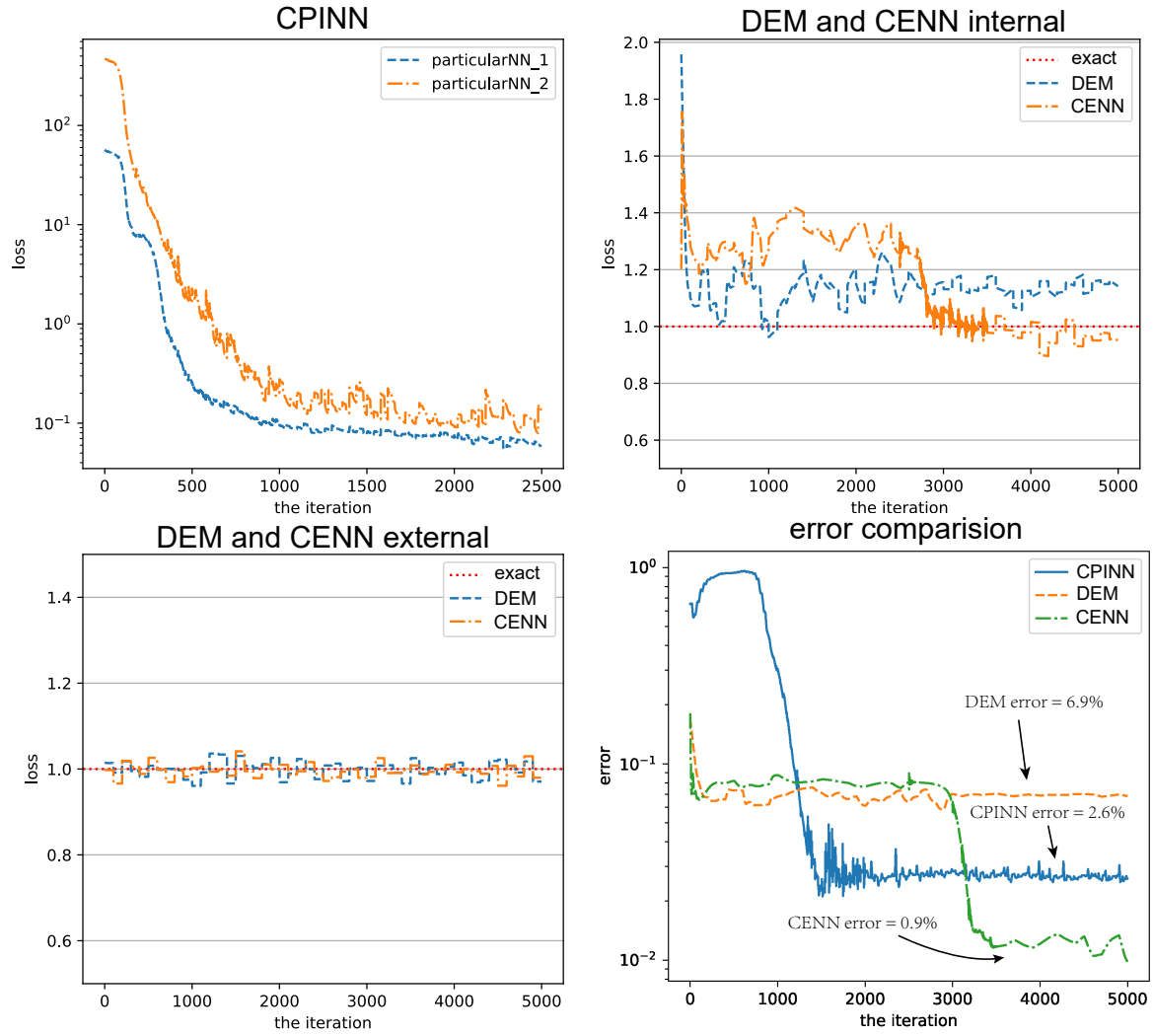


**Fig. 13.** Comparison of CPINN, DEM, and CENN in Koch: the loss function evolution of CPINN (upper left), comparison of the energy and the CENN loss function in the internal region with precise normalized functional integral (upper right), comparison of the energy and the CENN loss function in the external region with precise normalized functional integral (lower left), comparison of CPINN, energy, and CENN error (lower right)

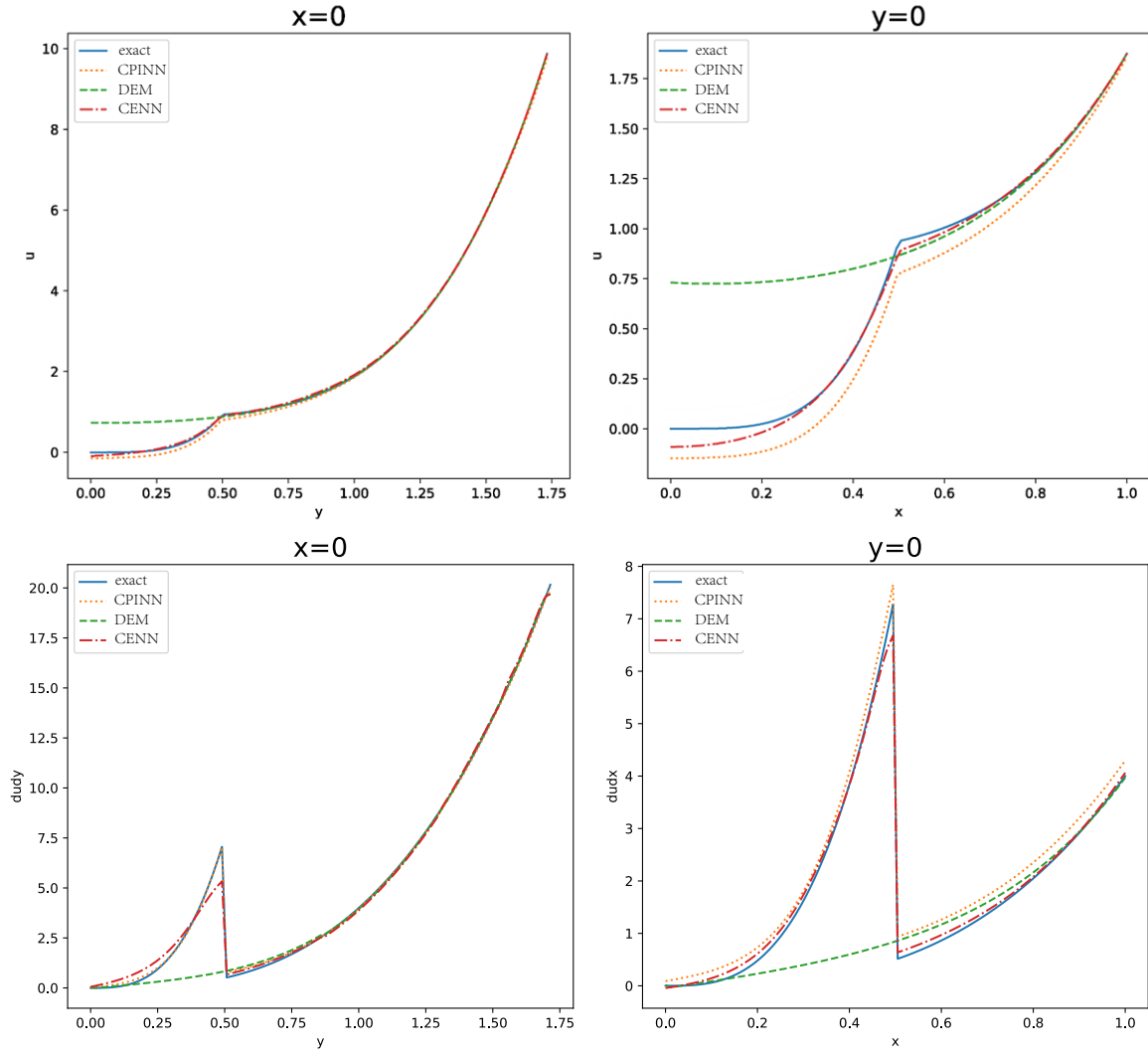


**Fig. 14.** Different location comparison of CPINN, DEM, and CENN in the Koch : Comparison of the displacement solution on the vertical line  $x=0$  (upper left), comparison of the displacement solution on the horizontal line  $y=0$  (upper right), comparison of the displacement derivative solution  $\frac{\partial u}{\partial r}$  on the vertical line  $x=0$  (lower left), comparison of the displacement solution  $\frac{\partial u}{\partial r}$  on the horizontal line  $y=0$  (lower right).

#### 4.3. Composite material hyperelasticity

In this section, we introduce hyperelasticity, which is a well-known problem including non-linear operator and vector-valued variables in solid mechanics. In [19], the homogeneous hyperelasticity problem is solved. We consider a body made of a nonhomogenous, i.e., composite hyperelastic material. The non-linear characteristic is from the large deformation and the hyperelastic constitutive law. The governing equation of the problem is

$$\begin{cases} \nabla_X \cdot P + f = 0 & x \in \Omega \\ u = \bar{u} & x \in \partial\Omega^{eb} \\ N \cdot P = \bar{t} & x \in \partial\Omega^{nb} \end{cases} \quad (30)$$

where  $\nabla_X$  is the gradient operator with respect to  $X$ ,  $X$  is material coordinate [30].  $\nabla_X \cdot P$  denotes the divergence operator, which we can use the tensor index to represent clearly  $\nabla_X \cdot P = P_{ij,i}$ .  $P$  is the Lagrange's stress, where the first component  $i$  and the second  $j$  of  $P_{ij}$  correspond the material coordinates and spatial coordinate respectively.  $f$  is the body force, and the first equation is the equilibrium equation in the domain  $\Omega$ . Note that  $P$  is the function of the material coordinate  $X$ .  $\bar{u}$  is the given displacement value in the essential boundary  $\partial\Omega^{eb}$ .  $N$  is the normal direction of the Newmann boundary  $\partial\Omega^{nb}$ , and  $\bar{t}$  is the prescribed traction on the Newmann boundary.

If the material is hyperelasticity,  $P$  can be written to the derivative of the strain energy  $\Psi$  with respect to the deformation gradient  $F$

$$P = \left( \frac{\partial \Psi}{\partial F} \right)^T \quad (31)$$

$$F = \frac{\partial x}{\partial X} \quad (32)$$

where the  $x = X + u(X)$  is the spatial coordinate, which is the function of the material coordinate  $X$ , given that it is a static problem independent of time.  $u$  is the interesting field, which in this specific problem is the vector displacement field. We consider the common used constitutive law Neo-Hookean of the hyperelasticity [31]

$$\Psi = \frac{1}{2} \lambda (\ln J)^2 - \mu \ln(J) + \frac{1}{2} \mu (\text{trace}(C) - 3) \quad (33)$$

where  $J$  is the determinant of the deformation gradient  $F$  and  $C$  is the Green tensor, i.e.,  $C = F^T F$ . The first and second terms of RHS respectively are incompressible condition and stress-free in the initial condition.  $\lambda$  and  $\mu$  is Lamé parameter

$$\begin{cases} \lambda = \frac{vE}{(1+v)(1-2v)} \\ \mu = \frac{E}{2(1+v)} \end{cases} \quad (34)$$

where  $E$  and  $v$  represent the elastic modulus and Poisson ratio respectively. The core of the problem is to obtain the displacement field  $u$ . There are two ways to do it. The first way is to solve the strong form Eq. (30) and the second way is to use the energy theory by optimizing the potential energy

$$Loss = \int_{\Omega} (\Psi - f) dV - \int_{\partial\Omega^{nb}} \bar{t} u dA \quad (35)$$

Noting that the trial function satisfies the essential boundary in advance. In Appendix C, we can find the implementation of strong form is more complicated than the energy form, and the highest derivative is higher than the energy form resulting in more computation cost and lower accuracy. For the sake of simplicity, we compare DEM and CENN. We use the finite element method as the reference solution.

We consider a two-dimensional bending beam made of the composite material, as shown in Fig. 15. The material parameter is, upper :  $E_0 = 1000, \mu_0 = 0.3$ , lower :  $E_1 = 10000, \mu_0 = 0.3$ . Finite element method as the reference solution divides the region into 400 (length)\*100 (height) quadratic elements for enough accurate reference solution. Fig. 15 shows the points distribution ways of the DEM and CENN. Training points are redistributed every 100 epochs in all methods. Because the given value on the essential boundary is zero, the

particular neural network is zero, i. e.,  $u_p = 0$ . In addition, given that the essential boundary geometry is simple, we can obtain the analytic solution of the distance function, i.e.,  $RBF(x, y) = x$  to ensure that the boundary conditions are exactly satisfied for the sake of simplicity. The structure of the generalized network is 4 layers, each layer has 20 neurons, and the learning rate is 0.001. We use LBFGS [32] as the optimizer. Given that the strain energy does not vary much from region to region, we optimize both neural networks in CENN not like the Koch example before. The neural network structure of DEM keeps the same as CENN for comparison. Fig. 16 shows the prediction of the FEM, DEM, and the CENN. We can find that the minimum displacement  $x$  and  $y$  of the CENN is more close to the reference solution, i.e. FEM. The pattern of DEM and CENN both coincides with FEM. This shows the prediction of DEM and CENN about original field  $u$  is both good overall. For further quantifying the error, we consider the relative error about displacement and Von-Mises stress related to the derivative of the displacement

$$Mises = \sqrt{\frac{3}{2} S^{dev} : S^{dev}} \quad (36)$$

where  $S$  is the Kirchhoff's stress

$$S = PF^{-T}. \quad (37)$$

and  $S^{dev}$  is the deviation tensor, i.e.,

$$S^{dev} = S - \frac{1}{3} \text{trace}(S)I. \quad (38)$$

Because of the different material parameters of the beam, the derivative of the displacement  $y$  with respect to the  $y$ -direction is discontinuous on the interface. Further, the Von-Mises is also discontinuous on the interface, so we consider the error  $||Von^{pred}|_2 - |Von^{fem}|_2|/|Von^{fem}|_2$  to consider the derivative error. Fig. 17 (left) shows the loss evolution of the CENN is much lower than the DEM. It is worth noting the optimal loss of the energy method is not zero due to obey the minimal potential theory. In some ways, the loss can reflect the accuracy of the method. Fig. 17 (mid) shows the relative error of CENN about displacement magnitude is 1.3 %, which is lower than DEM. The reason is that the derivative of displacement  $y$  w.r.t  $y$  direction is not continuity, so it is natural to divide the region according to the different materials to ease the restriction of derivative continuity. Fig. 17 (right) shows the relative error of CENN about Von-Mises stress is 0.11 %, which is very much smaller than DEM. Because CENN can better fit the derivative on the interface due to the inherent ability to simulate the discontinuity, the prediction about Von-Mises in CENN can be more close to the reference solution.

To further analyze the interface prediction of DEM and CENN, we compare the discontinuous derivative on the different vertical lines cross the interface,  $x=1$ ,  $x=2$ , and  $x=3$ , and we also compare the main deformation, i.e. displacement  $y$ , on the different horizontal line,  $y=0.25$ ,  $y=0.5$  and  $y=0.75$ . Fig. 18 (upper) shows the comparison of Von-Mises of DEM and CENN on the different vertical lines cross the interface,  $x=1$ ,  $x=2$ , and  $x=3$ . We can find CENN is more accurate than DEM in terms of discontinuous derivative. Fig. 18 (lower) shows the comparison of displacement  $y$  of DEM and CENN on the different horizontal lines,  $y=0.25$ ,  $y=0.5$ , and  $y=0.75$ . We can find both methods are good overall in terms of displacement  $y$ , but CENN is better.

## 5. Discussion

### 5.1. Discussion of admissible function errors

The above-mentioned data-driven and CENN error at the midpoint is larger than other points. Here we analyze the reason. We consider the derivative of the ring direction  $\theta$  at the center point.

$$\frac{\partial u(r, \theta; \theta_p, \theta_g)}{r \partial \theta} = \frac{\partial u_p(r, \theta; \theta_p)}{r \partial \theta} + \frac{\partial RBF(r, \theta)}{r \partial \theta} * u_g(r, \theta; \theta_g) + RBF(r, \theta) * \frac{\partial u_g(r, \theta; \theta_g)}{r \partial \theta}. \quad (39)$$

Here we assume that the RBF distance network is correct. It can be found in Fig. 5 (right), the result of the RBF distance network is consistent with the analytical solution. Therefore, this assumption is reasonable. Obviously, the RBF distance network in the Eq. (39) is equal to zero at the center point. At the same time, the RBF distance network keeps the same distance from the center point on the right half, as shown in Fig. 19, i.e.,

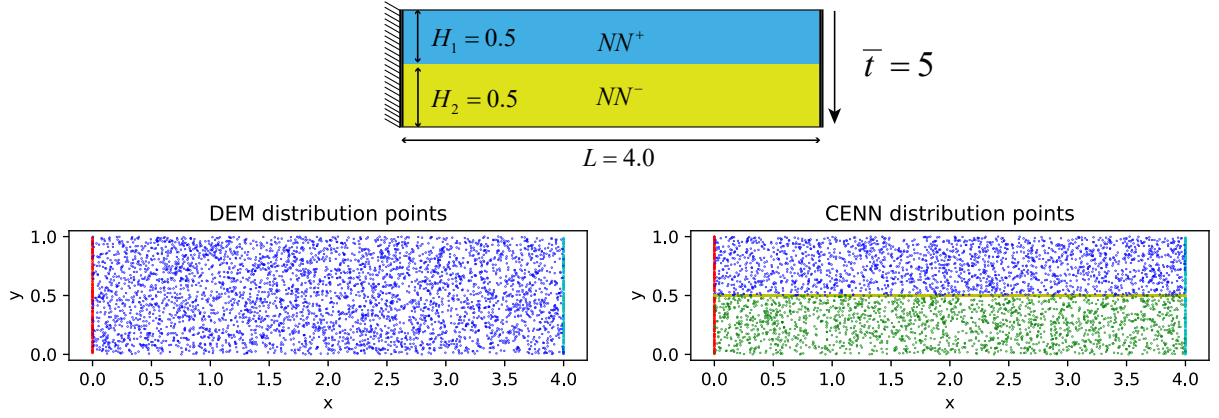


**Fig. 15.** The schematic diagram of the composite material beam, the blue and yellow stack denotes the different hyperelastic material, up:  $E_0 = 1000, \mu_0 = 0.3$ , down:  $E_1 = 10000, \mu_0 = 0.3$ , we use different neural networks corresponding to the different material. The length of the beam is 4 and the height of the beam is 1, the downward traction acting the right end of the beam is 5N and the left end of the beam is an essential fixed boundary (upper). Illustration of distribution points strategy of the DEM (lower left) and CENN (lower right), In DEM, the blue points are the domain training points of the neural network. In CENN, The blue points are the upper material training points of the neural network  $NN^+$ , the green points are the lower material training points of the neural network  $NN^-$ , the red points are the points of the essential boundary, and the yellow points are the interface points of the different materials. In both two energy ways, the total number of internal points is 4096, the number of essential boundary points is 256, and the number of interface points is 1000. All points are randomly distributed (lower)

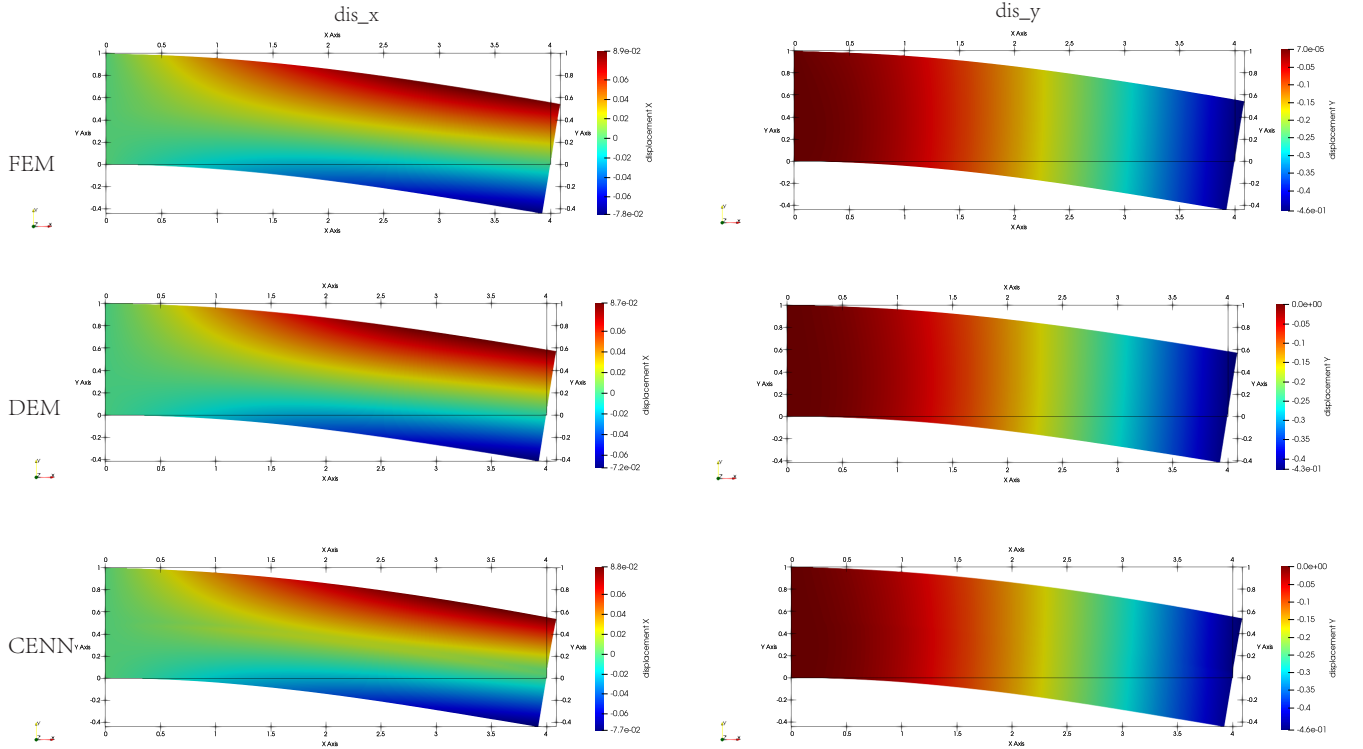


**Fig. 16.** Predicted solution by FEM, DEM, and CENN in beam: The displacement X field prediction result (left), the displacement Y field prediction result (right), FEM prediction (top row), DEM prediction (middle row), CENN prediction (bottom row).

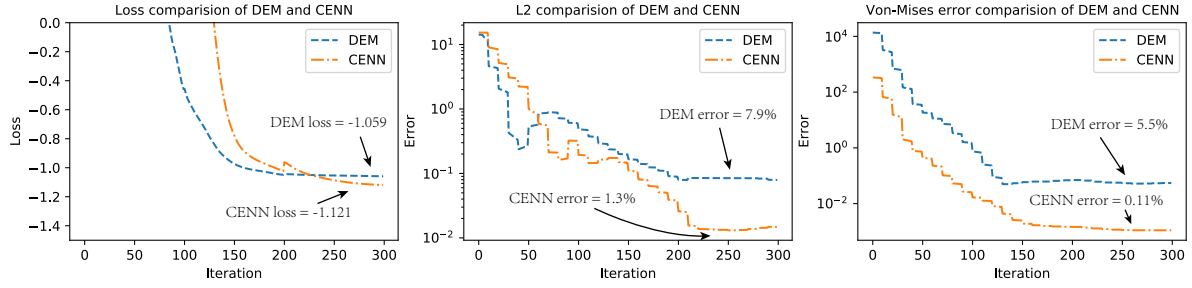


**Fig. 17.** Comparison of DEM and CENN in beam: the loss function evolution (left), relative error about displacement magnitude (mid), relative error about Von-Mises stress (right).

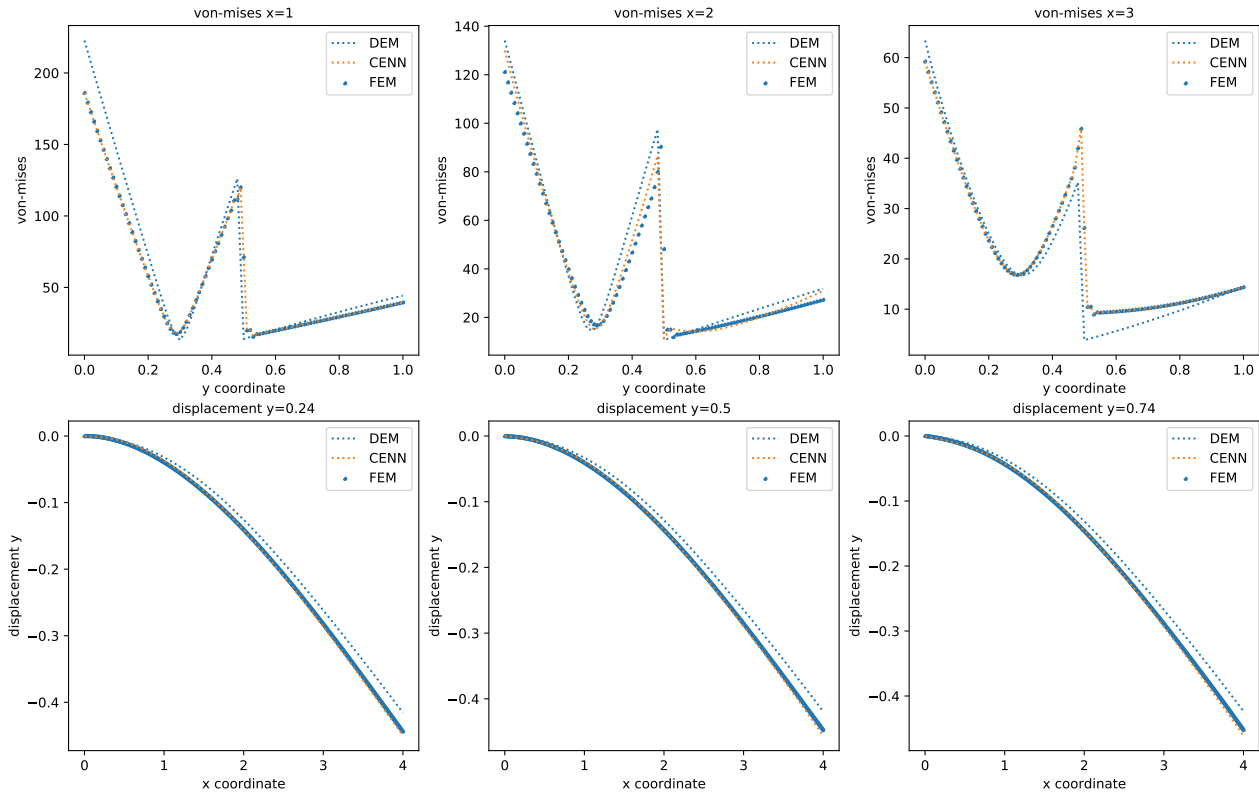


**Fig. 18.** Different location comparison of DEM and CENN in beam: Comparison of the Von-Mises solution on the different vertical line,  $x=1$ ,  $x=2$ ,  $x=3$  respectively (upper), comparison of the displacement  $y$  solution on the different horizontal line,  $y=0.25$ ,  $y=0.5$ ,  $x=0.75$  respectively (lower).



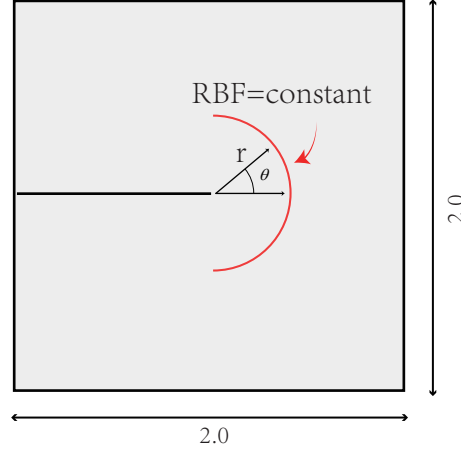


**Fig. 19.** RBF distance network constant diagram,  $r$  and  $\theta$  are standard polar coordinates, the prediction of RBF distance network is constant in the right half when  $r = \text{constant}$ , and the red line is the position where RBF prediction is constant

$\partial RBF(r, \theta)/r\partial\theta = 0$ . So when approaching the center point, we will get  $\partial RBF(r, \theta)/r\partial\theta = RBF(r, \theta) = 0$ , which will cause  $\partial u(r, \theta; \theta_p, \theta_g)/r\partial\theta = \partial u_p(r, \theta; \theta_p)/r\partial\theta$ . However we fixed the parameters of the particular network during training, so the energy density  $J_\rho = \frac{1}{2}[(\partial u/\partial r) + (\partial u/r\partial\theta)^2]$  at the center point can not be trained completely, i.e.,  $\partial u/r\partial\theta$  does not change, which leads to a large center point error. Fig. 7 (down left and right) shows that the error is mainly concentrated in the right half of the center point. This shortcoming can be overcome by changing the derivative term of the RBF distance network, i.e., change the form of the distance network to make  $\partial RBF(r, \theta)/r\partial\theta \neq 0$  at the center point. It will make training of the generalized network useful to perform learning further in the center. In another way, we can retrain the parameters of the particular network, but we need to add an additional penalty function to limit the change of the particular network parameters so that the energy density at the center point can be changed. This problem will be further studied in the future.

We consider the singular strain at  $x > 0, y = 0$ . Fig. 9 (down right) shows the greater the error when approaching  $x = 0$ . This is actually a special case of the above-mentioned hoop  $\theta$  derivative situation at the interface ( $x > 0, y = 0$ ),  $\partial u(r, \theta; \theta_p, \theta_g)/r\partial\theta = \partial u(x, y; \theta_p, \theta_g)/\partial y$ . It is also caused by the RBF distance network of the admissible function, we consider the derivative  $u$  w.r.t  $y$ -direction at the center point

$$\frac{\partial u(x, y; \theta_p, \theta_g)}{\partial y} = \frac{\partial u_p(x, y; \theta_p)}{\partial y} + \frac{\partial RBF(x, y)}{\partial y} * u_g(x, y; \theta_g) + RBF(x, y) * \frac{\partial u_g(x, y; \theta_g)}{\partial y}. \quad (40)$$

Obviously, the RBF distance network in Eq. (40) is equal to zero at the center point. In addition, we analyze  $x = \delta, y = 0$  at  $\partial RBF(x, y)/\partial y$ , Taylor series expand to second-order term

$$\begin{aligned} \frac{\partial R(y)}{\partial y} &= \lim_{d \rightarrow 0} \frac{\sqrt{\delta^2 + d^2} - \delta}{d} \\ &= \lim_{d \rightarrow 0} \frac{(\sqrt{\delta^2 + d^2} + \frac{\partial(\sqrt{\delta^2 + d^2})}{\partial y}|_{d=0}d + \frac{1}{2}\frac{\partial^2(\sqrt{\delta^2 + d^2})}{\partial^2 y}|_{\Delta=0}d^2 + o(d^2)) - \delta}{d} \\ &= \lim_{d \rightarrow 0} \frac{(\sqrt{\delta^2} + \frac{1}{2}\frac{1}{\delta}d^2 + o(d^2)) - \delta}{d} \\ &= 0 \end{aligned} \quad (41)$$

Where  $\delta$  is the distance from the center point (crack tip),  $\delta > 0$ , the coordinate point is  $(x = \delta, y = 0)$ , where  $d$  is the distance from the coordinate point to the  $x$ -axis, it is not difficult to found that the above derivative is always equal to 0 at  $x > 0, y = 0$ . So when approaching to the center point,  $\partial R(x, y)/\partial y = R(x, y) = 0$ , which

will lead to  $\partial u(x, y; \theta_p, \theta_g)/\partial y = \partial u_p(x, y; \theta_p)/\partial y$ , but during training, we fixed the parameters of the particular network, so the closer is to the center point, the more sensitive generalized network is.  $\partial u(x, y; \theta_p, \theta_g)/\partial y$  will have greater the error when approaching a center point.

### 5.2. The influence of point distribution on the solution

Different point allocation methods may affect the accuracy. At the same time, due to the constant of the distance network near the essential boundary, the generalized neural network near the essential boundary partially is very sensitive, resulting in increasing error. The sensitivity can be reduced by arranging more points around the center point.

The energy form depends more on the integration scheme because the loss function is the whole energy function, so the different ways of attribution points have a relatively large impact on the energy form. However, the strong form requires the error at the sampling point to be 0, so the requirement for the integration scheme is not high. It is worth noting that the overall loss function tends to be 0 in strong form, so the gradient descent has an impact to all the sampling points. In a way, the attribution ways have also an impact on the strong form. The impact of the attribution ways on the energy form is shown explicitly, while the impact of the attribution ways on the strong form is implicit.

### 5.3. Efficiency and accuracy

Since the admissible function requires additional training, the advanced training of the RBF distance network and the particular network will increase the additional computational cost. However, the traditional strong form does not need it, but the traditional strong form involves a higher-order derivative than the energy form, so the computational cost of the strong form is larger than the energy form after the admissible function training. This is a question of balance. In addition, higher-order derivatives will not only further increase the amount of the computational cost, but also affect the accuracy theoretically. It is worth noting that not all PDEs have a corresponding energy principle, so the generality of the energy principle is not as good as the strong form. At the same time, the energy principle requires more strict collocation methods due to the need for precise integration functionals, but the strong form does not have this restriction, and some batch methods can be used to improve convergence speed [16]. In addition, the choice of hyperparameters in traditional strong form is also a problem. Although there is NTK theory to automatically select hyperparameters [21, 22], accurate and quantitative optimal hyperparameters are still an important problem. Of course, the strong form can also use the construction of the admissible function to reduce the number of hyperparameters. If multiple neural network subdomains are involved, the hyperparameters about the interface will further increase greatly, and the interface loss term in CPINN will add the derivative term compared to the CENN. It will reduce the accuracy and efficiency. It is worth noting that there is no NTK theory of subdomains to automatically determine the hyperparameters, which will be further studied in the future.

### 5.4. Whether the generalized neural network is slicing

Considering that the interface is a continuous derivative in the crack, we do not actually need to slice the generalized network. But in some  $C_0$  problems (the original function is continuous, the first derivative is discontinuous), e.g. heterogeneous problem, the slicing of the generalized network is meaningful, which will be specifically illustrated in Section 4.2 with the complex boundary and Section 4.3.

We should consider the physical nature of the problem and thus decide whether to slice the neural network or not. The different regions are connected through the loss function.

## 6. Conclusion

We developed the CENN formulation based on the deep energy method to solve the heterogeneous partial differential equation. We showed the accuracy of the proposed method is higher than the DEM in terms of the heterogeneous problem, especially the derivative on the interface. We show the efficiency and accuracy of the proposed method CENN compared to the CPINN due to the lower-order derivative. The hyperparameter of the proposed method is far less than CPINN. We show CENN can solve the singularity strain problem, i.e.

crack, without special treatment such as finite crack element. We demonstrate why the PDE solution that uses neural networks as approximation functions can be successful from the perspective of trial functions as well as test functions. We proposed a method to construct the admissible function to solve the complex boundary problem, which extends the application range of the deep energy method. Further, we explore the ability of the proposed method to solve the hyperelasticity problem with heterogeneous material, high-order multi-physics, and vector-valued variables in solid mechanics. We show the ease of implementation of CENN compared to CPINN. We recommend the CENN if the heterogeneous PDE has the corresponding variational form because the accuracy and efficiency are better than CPINN and DEM.

Each region can be set individually in CENN, such as neural network structure, optimization method, and so on, this flexibility is a double-edged sword, the advantage is the freedom of choice, the disadvantage is that there is no optimal solution. A limitation of the proposed method is that the derivative w.r.t some direction on the essential boundary can not be learned well, which we will further study in the future. A limitation of this study is that the penalty of the interface is constructed by a heuristic algorithm, so the accurate quantity of the hyperparameter should be further studied in the future. An additional uncontrolled factor in almost scientific computation based deep learning is how to choose initial parameters, optimization way, neural network architecture, and so on. We believe the present paper is far from being the last word on the subject.

## References

- [1] E. Samaniego, C. Anitescu, S. Goswami, V. M. Nguyen-Thanh, H. Guo, K. Hamdia, X. Zhuang, T. Rabczuk, An energy approach to the solution of partial differential equations in computational mechanics via machine learning: Concepts, implementation and applications, *Computer Methods in Applied Mechanics and Engineering* 362 (2020) 112790.
- [2] G. E. Karniadakis, I. G. Kevrekidis, L. Lu, P. Perdikaris, S. Wang, L. Yang, Physics-informed machine learning, *Nature Reviews Physics* 3 (6) (2021) 422–440. doi:10.1038/s42254-021-00314-5.
- [3] J. Berg, K. Nyström, A unified deep artificial neural network approach to partial differential equations in complex geometries, *Neurocomputing* 317 (2018) 28–41.
- [4] O. C. Zienkiewicz, R. L. Taylor, J. Z. Zhu, *The finite element method: its basis and fundamentals*, Elsevier, 2005.
- [5] A. Krizhevsky, I. Sutskever, G. E. Hinton, Imagenet classification with deep convolutional neural networks, *Advances in neural information processing systems* 25 (2012) 1097–1105.
- [6] A. Graves, S. Fernández, F. Gomez, J. Schmidhuber, Connectionist temporal classification: labelling unsegmented sequence data with recurrent neural networks (2006) 369–376.
- [7] M. Popel, M. Tomkova, J. Tomek, L. Kaiser, J. Uszkoreit, O. Bojar, Z. Žabokrtský, Transforming machine translation: a deep learning system reaches news translation quality comparable to human professionals, *Nature communications* 11 (1) (2020) 1–15.
- [8] D. Silver, A. Huang, C. J. Maddison, A. Guez, L. Sifre, G. Van Den Driessche, J. Schrittwieser, I. Antonoglou, V. Panneershelvam, M. Lanctot, et al., *Mastering the game of go with deep neural networks and tree search*, *Nature* 529 (7587) (2016) 484–489, oA status: bronze. doi:10.1038/nature16961. URL <https://www.nature.com/articles/nature16961.pdf>
- [9] O. Vinyals, I. Babuschkin, W. M. Czarnecki, M. Mathieu, A. Dudzik, J. Chung, D. H. Choi, R. Powell, T. Ewalds, P. Georgiev, et al., Grandmaster level in starcraft ii using multi-agent reinforcement learning, *Nature* 575 (7782) (2019) 350–354. doi:10.1038/s41586-019-1724-z.
- [10] A. W. Senior, R. Evans, J. Jumper, J. Kirkpatrick, L. Sifre, T. Green, C. Qin, A. Žídek, A. W. Nelson, A. Bridgland, et al., Improved protein structure prediction using potentials from deep learning, *Nature* 577 (7792) (2020) 706–710. doi:10.1038/s41586-019-1923-7.
- [11] K. Hornik, M. Stinchcombe, H. White, Multilayer feedforward networks are universal approximators, *Neural networks* 2 (5) (1989) 359–366.
- [12] M. Raissi, P. Perdikaris, G. E. Karniadakis, Physics-informed neural networks: A deep learning framework for solving forward and inverse problems involving nonlinear partial differential equations, *Journal of Computational Physics* 378 (2019) 686–707.
- [13] H. Lee, I. S. J. J. o. C. P. Kang, Neural algorithm for solving differential equations 91 (1) (1990) 110–131.
- [14] A. D. Jagtap, E. Kharazmi, G. E. Karniadakis, Conservative physics-informed neural networks on discrete domains for conservation laws: Applications to forward and inverse problems, *Computer Methods in Applied Mechanics and Engineering* 365 (2020) 113028.
- [15] E. Kharazmi, Z. Zhang, G. E. Karniadakis, hp-vpinns: Variational physics-informed neural networks with domain decomposition, *Computer Methods in Applied Mechanics and Engineering* 374 (2021) 113547.
- [16] W. Li, M. Z. Bazant, J. Zhu, A physics-guided neural network framework for elastic plates: Comparison of governing equations-based and energy-based approaches, *Computer Methods in Applied Mechanics and Engineering* 383 (2021) 113933. doi:10.1016/j.cma.2021.113933.
- [17] H. Sheng, C. Yang, Pfn: A penalty-free neural network method for solving a class of second-order boundary-value problems on complex geometries, *Journal of Computational Physics* 428 (2021) 110085.

- [18] Z. Wang, Z. Zhang, A mesh-free method for interface problems using the deep learning approach, *Journal of Computational Physics* 400 (2020) 108963. [doi:10.1016/j.jcp.2019.108963](#).
- [19] V. M. Nguyen-Thanh, X. Zhuang, T. Rabczuk, A deep energy method for finite deformation hyperelasticity, *European Journal of Mechanics-A/Solids* 80 (2020) 103874.
- [20] E. Weinan, B. Yu, The deep ritz method: a deep learning-based numerical algorithm for solving variational problems, *Communications in Mathematics and Statistics* 6 (1) (2018) 1–12.
- [21] S. Wang, H. Wang, P. Perdikaris, On the eigenvector bias of fourier feature networks: From regression to solving multi-scale pdes with physics-informed neural networks, *Computer Methods in Applied Mechanics and Engineering* 384 (2021) 113938. [doi:10.1016/j.cma.2021.113938](#).
- [22] S. Wang, X. Yu, P. Perdikaris, When and why pinns fail to train: A neural tangent kernel perspective (2020).
- [23] S. Wang, Y. Teng, P. Perdikaris, Understanding and mitigating gradient pathologies in physics-informed neural networks, *arXiv preprint arXiv:2001.04536* (2020).
- [24] A. D. Jagtap, K. Kawaguchi, G. E. Karniadakis, Adaptive activation functions accelerate convergence in deep and physics-informed neural networks, *Journal of Computational Physics* 404 (2020) 109136. [doi:10.1016/j.jcp.2019.109136](#).
- [25] A. Paszke, S. Gross, S. Chintala, G. Chanan, E. Yang, Z. DeVito, Z. Lin, A. Desmaison, L. Antiga, A. Lerer, Automatic differentiation in pytorch (2017).
- [26] N. Ketkar, Introduction to pytorch, in: *Deep learning with python*, Springer, 2017, pp. 195–208.
- [27] D. P. Kingma, J. Ba, Adam: A method for stochastic optimization (2017).
- [28] X. Glorot, Y. Bengio, Understanding the difficulty of training deep feedforward neural networks, in: *Proceedings of the thirteenth international conference on artificial intelligence and statistics, JMLR Workshop and Conference Proceedings*, pp. 249–256.
- [29] S. Amini Niaki, E. Haghighat, T. Campbell, A. Poursartip, R. Vaziri, Physics-informed neural network for modelling the thermochemical curing process of composite-tool systems during manufacture, *Computer Methods in Applied Mechanics and Engineering* 384 (2021) 113959. [doi:10.1016/j.cma.2021.113959](#).
- [30] Y. Fung, *Foundations of solid mechanics*. 1965, Englewood Cliffs, NJ 436 (2010).
- [31] T. Belytschko, W. K. Liu, B. Moran, K. Elkhodary, *Nonlinear finite elements for continua and structures*, John wiley & sons, 2013.
- [32] I. Goodfellow, Y. Bengio, A. Courville, *Deep learning*, MIT press, 2016.

## Appendix A. Proof of Remark 3

For the sake of simplicity, we consider the Poisson equation with the whole essential boundary

$$\Delta u = f \quad (\text{A.1})$$

The energy form of the strong form is

$$Loss = \sum_{i=1}^{n^v} w_i w_\varepsilon(u_1(x_i; \theta)) - \sum_{i=1}^{n^v} w_i f_i u(x_i; \theta) \quad (\text{A.2})$$

where  $w_i$  is the weight of the attribution points  $x_i$ , especially  $w_i = V/n$  if uniform random Monte Carlo method is adopted.  $w_\varepsilon = \frac{1}{2}(\nabla u) \cdot (\nabla u)$ ,  $u$  is a scalar interesting variable. The first-order variation w. r. t. Loss is

$$\delta Loss = \sum_{i=1}^{n^v} \frac{V}{n} (\nabla u_i) \cdot (\nabla \delta u_i) - \sum_{i=1}^{n^v} \frac{V}{n} f_i \delta u_i \quad (\text{A.3})$$

The first term on the RHS is integrated by parts. We can get

$$\begin{aligned} \delta Loss &= \sum_{i=1}^{n^v} \frac{V}{n} (\Delta u_i) (\delta u_i) - \sum_{i=1}^{n^v} \frac{V}{n} f_i \delta u_i \\ &= \sum_{i=1}^{n^v} \frac{V}{n} (\Delta u_i - f_i) (\delta u_i) \end{aligned} \quad (\text{A.4})$$

Given the trial function  $u$  is an admissible function, the boundary part generated by integrating by parts with  $\delta u$  is vanish. Considering the interesting field  $u$  is the function of neural network parameter  $\theta$ , the variation

form can be rewritten

$$\begin{aligned}\delta Loss &= \sum_{i=1}^{n^v} \frac{V}{n} (\Delta u_i - f_i) \left( \sum_{j=1}^{n^\theta} \frac{\partial u_i}{\partial \theta_j} \delta \theta_j \right) \\ &= \sum_{j=1}^{n^\theta} \sum_{i=1}^{n^v} \frac{V}{n} (\Delta u_i - f_i) \left( \frac{\partial u_i}{\partial \theta_j} \delta \theta_j \right)\end{aligned}\tag{A.5}$$

The stationary point, i.e. the end of the optimization by gradient, is equal to the strong form with the test function  $\partial u(x; \theta) / \partial \theta_j$ ,  $j=1, 2, \dots, n^\theta$ , i. e. ,

$$\begin{aligned}Loss_1 &= \sum_{i=1}^{n^v} \frac{V}{n} (\Delta u_i - f_i) \left( \frac{\partial u_i}{\partial \theta_1} \right) \\ Loss_2 &= \sum_{i=1}^{n^v} \frac{V}{n} (\Delta u_i - f_i) \left( \frac{\partial u_i}{\partial \theta_2} \right) \\ &\vdots \\ Loss_{n^\theta} &= \sum_{i=1}^{n^v} \frac{V}{n} (\Delta u_i - f_i) \left( \frac{\partial u_i}{\partial \theta_{n^\theta}} \right)\end{aligned}\tag{A.6}$$

DEM can be thought of as jointly optimizing all the above losses so that all losses converge to zero.

On the other hand, we analyze the traditional PINN, i.e., the least square method

$$Loss = \sum_{i=1}^{n^v} \frac{V}{n} (\Delta u_i - f_i)^2.\tag{A.7}$$

The first-order variation w.r.t. PINN loss is

$$\delta Loss = \sum_{i=1}^{n^v} \frac{V}{n} 2(\Delta u_i - f_i) (\Delta \delta u_i).\tag{A.8}$$

Considering the interesting field  $u$  is the function of neural network parameter  $\theta$ , we can obtain

$$\delta Loss = \sum_{j=1}^{n^\theta} \sum_{i=1}^{n^v} \frac{V}{n} 2(\Delta u_i - f_i) \left( \Delta \frac{\partial u_i}{\partial \theta_j} \delta \theta_j \right).\tag{A.9}$$

The traditional PINN is equal to the strong form with the test function  $2\Delta \frac{\partial u}{\partial \theta_j}$ ,  $j=1, 2, \dots, n^\theta$ , i.e.,

$$\begin{aligned}Loss_1 &= \sum_{i=1}^{n^v} \frac{V}{n} (\Delta u_i - f_i) \left( 2\Delta \frac{\partial u_i}{\partial \theta_1} \right) \\ Loss_2 &= \sum_{i=1}^{n^v} \frac{V}{n} (\Delta u_i - f_i) \left( 2\Delta \frac{\partial u_i}{\partial \theta_2} \right) \\ &\vdots \\ Loss_{n^\theta} &= \sum_{i=1}^{n^v} \frac{V}{n} (\Delta u_i - f_i) \left( 2\Delta \frac{\partial u_i}{\partial \theta_{n^\theta}} \right)\end{aligned}\tag{A.10}$$

Traditional PINN can be thought of as jointly optimizing all the above losses so that all losses converge to zero.

So the test function of DEM is  $\partial u(x; \theta) / \partial \theta_j$ , the test function of traditional PINN is  $2\Delta \partial u / \partial \theta_j$ . Because DEM pay more attention to the first derivative of the interesting field, the derivative result is better than PINN. In fact, both of these are actually special cases of the weighted residual method.

If the second-order coordinate derivative of the interesting field is not close to zero, though first-order derivative close to zero, e.g., the minimum value problem, the strong form may be better than energy form because test function is not zero compared to energy form.

## Appendix B. Back propogation of CENN

We consider the energy form of CENN

$$\begin{aligned} Loss = & \sum_{i=1}^{n_1} w_i w_\varepsilon(u_1(x_i; \theta_1)) - \sum_{i=1}^{n_1} w_i f_i u_1(x_i; \theta_1) \\ & + \sum_{i=1}^{n_2} w_i w_\varepsilon(u_2(x_i; \theta_2)) - \sum_{i=1}^{n_2} w_i f_i u_2(x_i; \theta_2) \\ & + \frac{penalty}{n_{inter}} \sum_{i=1}^{n_{inter}} (u_1(x_i; \theta_1) - u_2(x_j; \theta_2))^2 \end{aligned} \quad (B.1)$$

where  $w_i$  is the weight of the attribution points  $x_i$ , especially  $w_i = V/n$  if uniform random Monte Carlo method is adopted.  $w_\varepsilon$  is the strain energy density,  $u_1$  and  $u_2$  is interesting variable according to the different subdomains.  $f_i$  is the body force w.r.t. the point  $x_i$ .  $\theta_1$  and  $\theta_2$  are neural network parameters according to the different subdomains. The last term on RHS is the continuity condition on the interface by the MSE criterion.

Back propagate Eq. (B.1) to find the derivative of the loss function with respect to parameters of neural network 1

$$\begin{aligned} \frac{\partial Loss}{\partial \theta_1} = & \sum_{i=1}^{n_1} w_i \frac{\partial w_\varepsilon(u_1(x_i; \theta_1))}{\partial u_1(x_i; \theta_1)} \frac{\partial u_1(x_i; \theta_1)}{\partial \theta_1} - \sum_{i=1}^{n_1} w_i f_i \frac{\partial u_1(x_i; \theta_1)}{\partial \theta_1} \\ & + \frac{penalty}{n_{inter}} \sum_{i=1}^{n_{inter}} 2(u_1(x_i; \theta_1) - u_2(x_j; \theta_2)) \frac{\partial u_1(x_i; \theta_1)}{\partial \theta_1} \end{aligned} \quad (B.2)$$

If we consider the one dimension elastic problem, the strain energy density is

$$w_\varepsilon(u(x_i; \theta)) = \frac{1}{2} E \left( \frac{\partial u(x; \theta)}{\partial x} \Big|_{x=x_i} \right)^2 \quad (B.3)$$

We substitute the strain energy density to Eq. (B.2), we can obtain

$$\begin{aligned} \frac{\partial Loss}{\partial \theta_1} = & \sum_{i=1}^{n_1} w_i E \frac{\partial u_1(x; \theta_1)}{\partial x} \Big|_{x=x_i} \frac{\partial \left( \frac{\partial u_1(x; \theta_1)}{\partial x} \Big|_{x=x_i} \right)}{\partial \theta_1} - \sum_{i=1}^{n_1} w_i f_i \frac{\partial u_1(x_i; \theta_1)}{\partial \theta_1} \\ & + \frac{penalty}{n_{inter}} \sum_{i=1}^{n_{inter}} 2(u_1(x_i; \theta_1) - u_2(x_j; \theta_2)) \frac{\partial u_1(x_i; \theta_1)}{\partial \theta_1} \end{aligned} \quad (B.4)$$

Here we use the chain rule to get

$$\frac{\partial u_1(x; \theta_1)}{\partial x} \Big|_{x=x_i} = \left( \frac{\partial u}{\partial z^{(L+1)}} \frac{\partial z^{(L+1)}}{\partial a^{(L)}} \right) \left( \frac{\partial a^{(L)}}{\partial z^{(L)}} \frac{\partial z^{(L)}}{\partial a^{(L-1)}} \right) \dots \left( \frac{\partial a^{(2)}}{\partial z^{(2)}} \frac{\partial z^{(2)}}{\partial a^{(1)}} \right) \left( \frac{\partial a^{(1)}}{\partial z^{(1)}} \frac{\partial z^{(1)}}{\partial x} \right) \quad (B.5)$$

where  $a^{(M)}$  and  $z^{(M)}$  is an activation neuron (act by the activation function) and a linear neuron (not through an activation function),  $M = 1, 2, \dots, L$ ,  $L$  is the hidden layer of the neural network. The derivative term is

$$\frac{\partial a^{(L)}}{\partial z^{(L)}} = \text{diag}(\sigma'^{(L)}|_{z^{(L)}}) \quad (\text{B.6})$$

where  $\text{diag}(\sigma'^{(L)}|_{z^{(L)}})$  denotes that the diagonal element is  $\sigma'_i{}^{(L)}$ ,  $i = 1, 2, \dots, L_n$ ,  $L_n$  is the number of the neuron in layer  $L$ . Another derivative term is

$$\frac{\partial z^{(L+1)}}{\partial a^{(L)}} = W^{(L+1)} \quad (\text{B.7})$$

where  $W$  is the weight of the layer  $L + 1$ , We obtain a more detailed expression of Eq. (B.5)

$$\frac{\partial u_1(x; \theta_1)}{\partial x} \Big|_{x=x_i} = [W^{(L+1)}][\text{diag}(\sigma'^{(L)}|_{z^{(L)}}) \cdot W^{(L)}] \dots [\text{diag}(\sigma'^{(2)}|_{z^{(2)}}) \cdot W^{(2)}][\text{diag}(\sigma'^{(1)}|_{z^{(1)}}) \cdot W^{(1)}] \quad (\text{B.8})$$

$$\frac{\partial u_1(x; \theta_1)}{\partial \theta_1^{(r)}} \Big|_{x=x_i} = [W^{(L+1)}][\text{diag}(\sigma'^{(L)}|_{z^{(L)}}) \cdot W^{(L)}] \dots [\text{diag}(\sigma'^{(r)}|_{z^{(r)}}) \cdot I_{r_n} \otimes a^{(r-1)}] \quad (\text{B.9})$$

It is worth noting that, in general, the last layer has no activation function, so  $\text{diag}(\sigma'^{(L+1)}|_{z^{(L+1)}}) = 1$ . So the term in Eq. (B.4) is

$$\begin{aligned} \frac{\partial(\frac{\partial u(x; \theta)}{\partial x} \Big|_{x=x_i})}{\partial \theta_w^{(r)}} &= [W^{(L+1)}][\text{diag}(\sigma'^{(L)}|_{z^{(L)}}) \cdot W^{(L)}] \\ &\dots [\text{diag}(\sigma'^{(r)}|_{z^{(r)}}) \otimes [\text{diag}(\sigma'^{(r-1)}|_{z^{(r-1)}}) \cdot W^{(r-1)}] \\ &\dots [\text{diag}(\sigma'^{(2)}|_{z^{(2)}}) \cdot W^{(2)}][\text{diag}(\sigma'^{(1)}|_{z^{(1)}}) \cdot W^{(1)}] \end{aligned} \quad (\text{B.10})$$

where  $\otimes$  denotes the merge action the tensor, so the derivative of the loss function with respect to the parameters can be expressed as

$$\begin{aligned} \frac{\partial \text{Loss}}{\partial \theta_w^{(r)}} &= \sum_{i=1}^{n_1} w_i E\{[W^{(L+1)}][\text{diag}(\sigma'^{(L)}|_{z^{(L)}}) \cdot W^{(L)}] \dots [\text{diag}(\sigma'^{(2)}|_{z^{(2)}}) \cdot W^{(2)}][\text{diag}(\sigma'^{(1)}|_{z^{(1)}}) \cdot W^{(1)}]\} \Big|_{x=x_i} \\ &\cdot \{[W^{(L+1)}][\text{diag}(\sigma'^{(L)}|_{z^{(L)}}) \cdot W^{(L)}] \dots [\text{diag}(\sigma'^{(r)}|_{z^{(r)}}) \otimes [\text{diag}(\sigma'^{(r-1)}|_{z^{(r-1)}}) \cdot W^{(r-1)}] \\ &\dots [\text{diag}(\sigma'^{(2)}|_{z^{(2)}}) \cdot W^{(2)}][\text{diag}(\sigma'^{(1)}|_{z^{(1)}}) \cdot W^{(1)}]\} \Big|_{x=x_i} - \sum_{i=1}^{n_1} w_i f_i \{[W^{(L+1)}][\text{diag}(\sigma'^{(L)}|_{z^{(L)}}) \cdot W^{(L)}] \\ &\dots [\text{diag}(\sigma'^{(r)}|_{z^{(r)}}) \cdot I_{r_n} \otimes a^{(r-1)}]\} \Big|_{x=x_i} + \frac{\text{penalty}}{n_{\text{inter}}} \sum_{i=1}^{n_{\text{inter}}} 2(u_1(x_i; \theta_1) - u_2(x_j; \theta_2)) \\ &[W^{(L+1)}][\text{diag}(\sigma'^{(L)}|_{z^{(L)}}) \cdot W^{(L)}] \dots [\text{diag}(\sigma'^{(r)}|_{z^{(r)}}) \cdot I_{r_n} \otimes a^{(r-1)}] \end{aligned} \quad (\text{B.11})$$

The neural network 2 is the same as the neural network 1.

### Appendix C. The strong form of the hyperelasticity

In the section, we derive the strong form of hyperelasticity with respect to Neo-Hookean. The strong form is



$$\begin{cases} \nabla_X \cdot P + f = 0 & x \in \Omega \\ u = \bar{u} & x \in \partial\Omega^{eb} \\ N \cdot P = \bar{t} & x \in \partial\Omega^{nb} \end{cases} \quad (C.1)$$

where  $P = (\frac{\partial\Psi}{\partial F})^T$  and  $\Psi = \frac{1}{2}\lambda(\ln J)^2 - u\ln(J) + \frac{1}{2}u(\text{trace}(C) - 3)$ , so we can use the chain derivative to get

$$P = \left( \frac{\partial\Psi}{\partial J} \frac{\partial J}{\partial F} + \frac{\partial\Psi}{\partial \text{trace}(C)} \frac{\partial \text{trace}(C)}{\partial C} \frac{\partial C}{\partial F} \right)^T \quad (C.2)$$

Further, we can use the tensor derivative to get

$$\begin{cases} \frac{\partial J}{\partial F} = JF^{-T} \\ \frac{\partial \text{trace}(C)}{\partial C} = I \\ \frac{\partial C_{ij}}{\partial F_{mn}} = \delta_{in}F_{mj} + F_{mi}\delta_{jn} \end{cases} \quad (C.3)$$

We substitute Eq. (C.3) to Eq. (C.2), we can obtain

$$P = \mu F^T + [\lambda \ln(J) - \mu] F^{-1} \quad (C.4)$$

where

$$F = \frac{\partial x}{\partial X} = I + \frac{\partial u(X)}{\partial X} \quad (C.5)$$

Finally, we get the strong form with respect to the  $u$

$$\begin{cases} \nabla_X \cdot \left\{ \mu \left( I + \frac{\partial u(X)}{\partial X} \right)^T + [\lambda \ln(J) - \mu] \left( I + \frac{\partial u(X)}{\partial X} \right)^{-1} \right\} + f = 0 & x \in \Omega \\ u = \bar{u} & x \in \partial\Omega^{eb} \\ N \cdot \left\{ \mu \left( I + \frac{\partial u(X)}{\partial X} \right)^T + [\lambda \ln(J) - \mu] \left( I + \frac{\partial u(X)}{\partial X} \right)^{-1} \right\} = \bar{t} & x \in \partial\Omega^{nb} \end{cases} \quad (C.6)$$

We can find the strong form is more complicated than the energy form.